

Research Article

Late Quaternary fluvial and aeolian depositional environments for the western Red River, Southern Great Plains, USA

Steven L. Forman^{a*}, Zequn Wu^a, Logan Wiest^b, Liliana Marin^a and Connor Mayhack^a

^aDepartment of Geosciences, Baylor University, Waco, TX 76798, USA and ^bDepartment of Natural Sciences, Mansfield University 205B Belknap Hall, 31 South Academy Street, Mansfield, PA 16933, USA

Abstract

Ubiquitous Holocene dune systems are associated with major west-to-east flowing rivers across the Southern Great Plains (SGP), USA. Critical questions remain as to whether aeolian activity reflects multiple environmental signatures, including increased sand supply from riverine sources. This research focused on the western Red River where geomorphic mapping revealed three terrace levels up to 16 m, buried partially by up to 10 m of aeolian sediments. Pedosedimentary facies analyses of sections and Geoprobe cores extracted from terraces and close-interval optically stimulated luminescence dating of quartz grains revealed two periods of fluvial aggradation at ca. 80 ka to ~5 to 8 m above the Red River forming the Vernon terrace, and at 30 to 13 ka to ~20–15 m, the highest identified Childress terrace. Net degradation of 20 m also occurred between 13 and 7 ka to 4 m below the current channel, reflecting regional fall in the groundwater level. The latest aggradation event, which built the lowest Luna terrace at ~2 m, ended 1.5 to 0.7 ka and was partially buried by fluvial-sourced dunes in the sixteenth and seventeenth centuries. This recent phase of aeolian deposition coincides with a comparatively wet period in the central United States during the Little Ice Age, rather than with regional drying.

Keywords: Fluvial terraces, Dunes, Little Ice Age, OSL ages, Fluvial–aeolian dynamics, Holocene, Late Pleistocene

(Received 12 November 2022; accepted 21 March 2023)

INTRODUCTION

Vast aeolian systems occur adjacent to west-to-east flowing rivers across the Southern Great Plains (SGP) (Fig. 1), have repeatedly reactivated in the Holocene, and are potentially significant sources of dust for adjacent metropolitan centers (e.g., Routson et al., 2016; Bolles et al., 2019; Sweeney et al., 2022). This area where stabilized and active dune systems abound is characterized by moderate to high wind drift potential, with assumed threshold wind speeds of 5 to 6 m/s for aeolian entrainment (Schmeisser et al., 2010), though higher wind thresholds of ≥ 10 m/s may be needed on crusted or vegetated surfaces to initiate saltation (Bolles et al., 2019; Sweeney et al., 2022). Foundational studies indicate abundant aeolian sediment sources from preexisting aeolian deposits and active fluvial systems on the SGP (e.g., Holliday, 1995; Muhs, 2017). Often, sediment sources and availability are enhanced by a paucity of stabilizing vegetation (i.e., reduced below a coverage threshold of ~40%) that may occur with multiyear to decadal-scale severe droughts or megadroughts (e.g., Forman et al., 2001; Mangan

et al., 2004; Stahle et al., 2007; Cook et al., 2016). However, critical questions remain concerning whether dune reactivation on the Great Plains reflects a response to drought variability or more stochastic processes associated with grassland response to varying moisture availability, long stabilization times, grazing disturbance, and edaphic processes (e.g., Luna et al., 2011; Werner et al., 2011; Barchyn and Hugenholtz, 2012; Hugenholtz and Koenig, 2014; Halfen et al., 2016).

A significant source for aeolian sediments during periods of dune expansion or accretion may be from fluvial systems in this semiarid environment (e.g., Kocurek and Lancaster, 1999; Lancaster and Tchakerian, 2003; Wright et al., 2011; Halfen et al., 2016; Sankey et al., 2018). Specifically, braided reaches or broad exposed floodplains may originate source-border dunes on the adjacent floodplain or fluvial terraces (Draut, 2012; Liu and Coulthard, 2015; Sankey et al., 2018). Rivers can be also barriers to sand dune migration, as shown by the Colorado River impeding sand transport from the Mojave Desert (Muhs et al., 2003; Draut, 2012). Flood deposits of dryland rivers can be aeolian sediment sources (Bullard and McTainsh, 2003; Sankey et al., 2018). The influence of abundant flood-derived sediments on aeolian source zones can persist tens to hundreds of kilometers downwind along a river (e.g., Muhs et al., 2003; Alizai et al., 2011). In turn, fluvial degradation and channel migration may perch dune fields above the active river channel. These aeolian

*Corresponding author at: Department of Geosciences, Baylor University, Waco, TX 76798, USA. E-mail address: Steven_Forman@Baylor.edu (S.L. Forman).

Cite this article: Forman SL, Wu Z, Wiest L, Marin L, Mayhack C (2023). Late Quaternary fluvial and aeolian depositional environments for the western Red River, Southern Great Plains, USA. *Quaternary Research* 115, 3–24. <https://doi.org/10.1017/qua.2023.15>



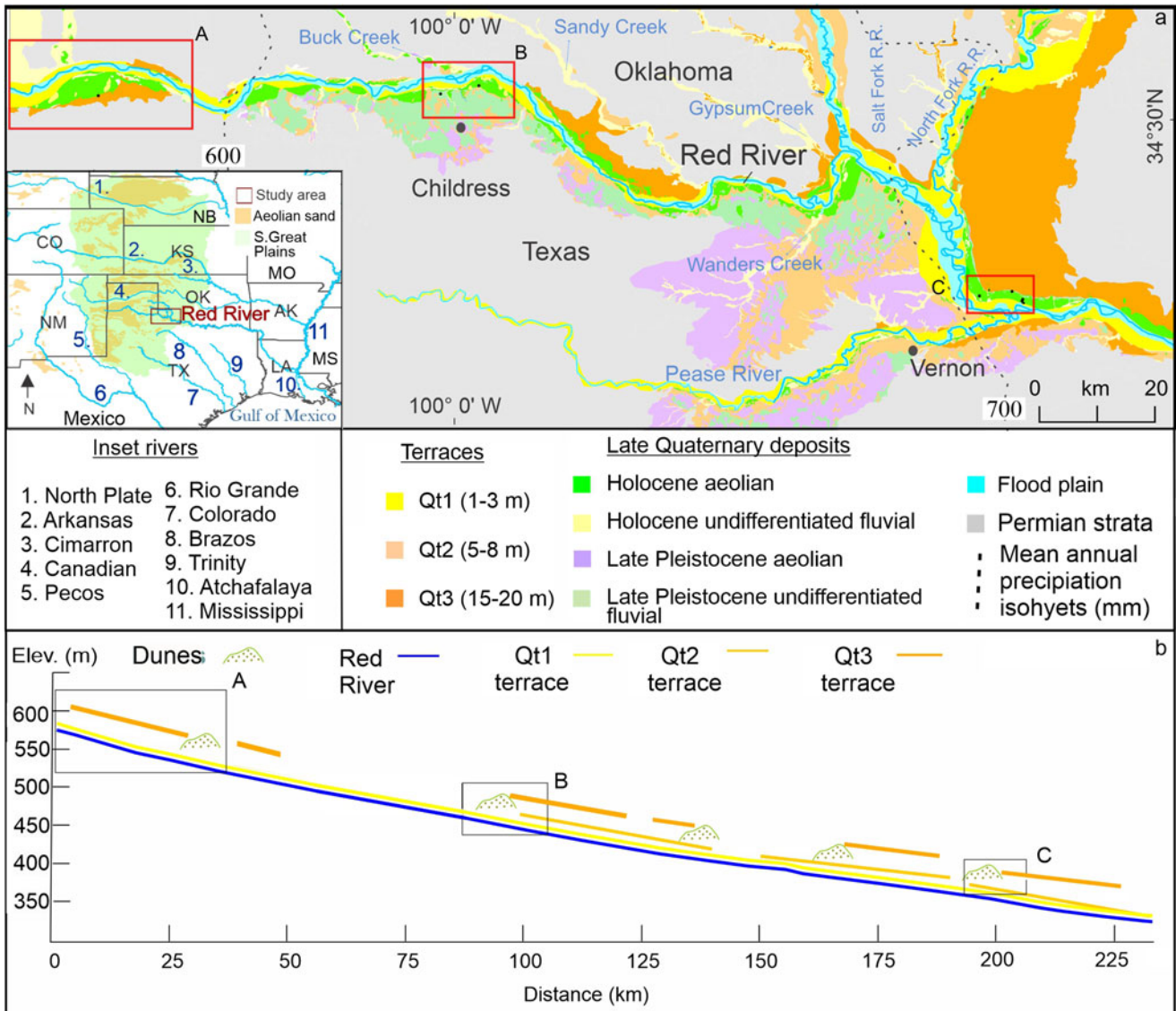


Figure 1. (a) Western Red River at Texas and Oklahoma border in the eastern edge of Southern Great Plains (inset) showing current channel; floodplain; Qt1, Qt2, and Qt3 terraces; and surficial Late Quaternary deposits. Dashed line indicates mean annual precipitation isohyets, with study area mostly between 600 and 700 mm. Red boxes labeled A, B, and C indicate study areas shown in Fig. 2. (b) Diagrammatic cross-section for the length of part a showing the Red River; Qt1, Qt2, and Qt3 terraces; and major dunes.

systems may be partially or wholly isolated from riverine sediment sources, and with a fall in the water table, vegetation may shift to drier C_4 grassland species and lower the threshold for dune reactivation with drying (e.g., Forman et al., 2001; Mangan et al., 2004; Houser et al., 2015).

There is compelling evidence for multiple aeolian depositional events in the past 2000 yr for many dune fields adjacent to major drainages on the SGP (e.g., Forman et al., 2001, 2008; Werner et al., 2011; Halfen and Johnson, 2013). However, there is considerable uncertainty surrounding the asynchrony of aeolian systems' activity and times of stability across the SGP, reflecting a number of factors, including varying sediment supply and availability, threshold wind speeds, hydrologic and climatic variability, lagged aeolian system response, stratigraphic incompleteness, and the limited number of detailed chronostratigraphic studies spanning the Holocene (e.g., Holliday, 2001; Forman et al., 2008, 2022; Halfen, 2012; Halfen and Johnson,

2013; Halfen et al., 2016). Dune fields adjacent to the Arkansas River in west Kansas revealed a sequence of aeolian sands intercalated with weak buried soils that yielded optically stimulated luminescence (OSL) ages reflecting sand sheet accretion at ca. 1490 to 1250, 430, 380 to 320, 180, and 70 yr ago (Forman et al., 2008). Three broad periods of aeolian accretion at ca. 2100 to 1800, 1000 to 900, and 600 to 70 yr were inferred for the Hutchinson dunes in east-central Kansas based on OSL dating of strata (Halfen et al., 2012). In contrast, large, stabilized dune ridges on the second terrace of the Cimarron River yielded OSL ages between 880 and 770 yr (Lepper and Scott, 2005). Significant aeolian erosion on upland surfaces adjacent to the Cimarron River bend area (in Kansas and Oklahoma) is indicated by large deflation hollows infilled by sand sheet-type strata spanning from 810 to 460 yr (Werner et al., 2011). OSL dating of paleosurfaces preserved beneath fence-line deposits near the Canadian River in northwest Oklahoma revealed aeolian

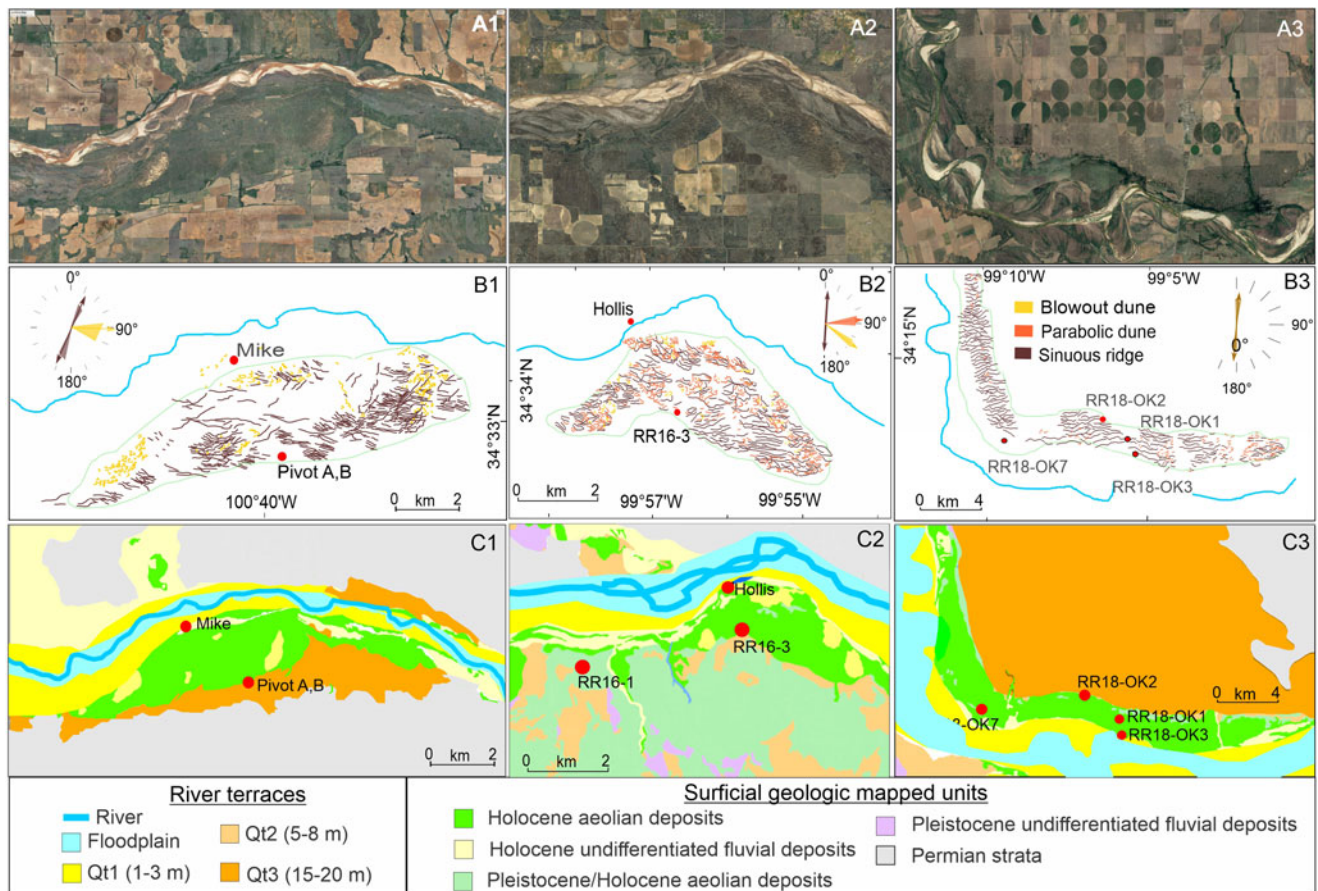


Figure 2. Geomorphic forms for study areas A–C as shown on Fig. 1. Subfigures A1, B1 and C1 are Google Earth images derived from aerial photographs (May 2016). Subfigures A2, B2, and C2 are line drawings showing distribution of aeolian landforms for the most recent blowout dunes (yellow) and older parabolic dunes (orange) accreted from winds from the west to northwest, with most common sinuous ridges (dark brown) showing the north–south sense of these oldest landforms. The directionality of aeolian landforms is detailed by the inset directional roses, with color (yellow, orange, and dark brown) reflecting corresponding mapped aeolian landforms (blowout dune, parabolic dune, and sinuous ridge). Subfigures A3, B3, and C3 show detailed mapping of terraces and surficial deposits in reference to location of stratigraphic sites and Geoprobe cores (RR18- or RR16-) from Fig. 1.

deposition at ca. 215 yr ago, before cultivation, with overlying sands from the twentieth century Cordova et al. 2005). Soils and ^{14}C ages from the Southern High Plains indicate spatial discontinuous occurrence of sand sheets ca. 1000 to 500 cal yr BP, with stability soon after and additional sand sheet deposition at 500 to 300 cal yr BP (Holliday, 2001). Radiocarbon ages of buried A horizons at the Muleshoe dune field in west Texas provide maximum limiting ages on soil burial by aeolian sand at ca. ~1300, 750 to 670, and ~500 cal yr BP (Holliday, 2001). The Mescalero sand sheet in southeastern New Mexico buried a sub-jacent paleosol and yielded a basal OSL age of 620 yr (Hall and Goble, 2012). At the surface, coppice and parabolic dunes abound and may reflect anthropogenic disturbance since the nineteenth century (Hall and Goble, 2012). This study focuses on deciphering the fluvial and aeolian geomorphic and stratigraphic record along the upper reach of the Red River, west of the confluence with the Pease River (Figs. 1 and 2). We delineate the possible fluvial–aeolian depositional pathways for formation of source-border dune fields with climate variability in the past ca. 600 yr. Geoprobe cores, 5 to 15 m long, allow close-interval OSL dating of quartz grains through surface-forming aeolian deposits and underlying terraces that reveals significant time (10^3 to 10^4 yr scales) unconformities.

CLIMATIC AND GEOMORPHIC CONTEXT OF THE WESTERN RED RIVER, TX-OK BORDER

The Red River flows across a significant moisture gradient, with mean annual precipitation (MAP) of 400 mm near its headwaters at 1050 m above sea level (m asl) elevation in west Texas and adjacent New Mexico to 1500 mm MAP at its point of discharge in eastern Louisiana into the Atchafalaya River at 25 m asl (Bertrand and McPherson, 2018). In west Texas, this river flows across Permian carbonate lithologies, gray sandstones, and red shales and sandstones; suspended sediment from these last lithologies is the presumed source of the red color. The high variance in discharge of the Red River exemplifies twentieth- and twenty-first-century climate variability on the SGP, with often-dry bed conditions during droughts between 2008 and 2014; extreme flood events in wetter years, as in 2015; and longer dry periods projected by 2050 (Qiao et al., 2017; Bertrand and McPherson, 2018). Discharge of the western Red River becomes intermittent during drought conditions, with net transmission loss through channel infiltration (Bertrand and McPherson, 2018; Huggins et al., 2022; Zipper et al., 2022) and broad exposure of the valley train for aeolian reworking.

The wind climate of the western Red River, defined in this study using wind velocity and direction data for the Childress

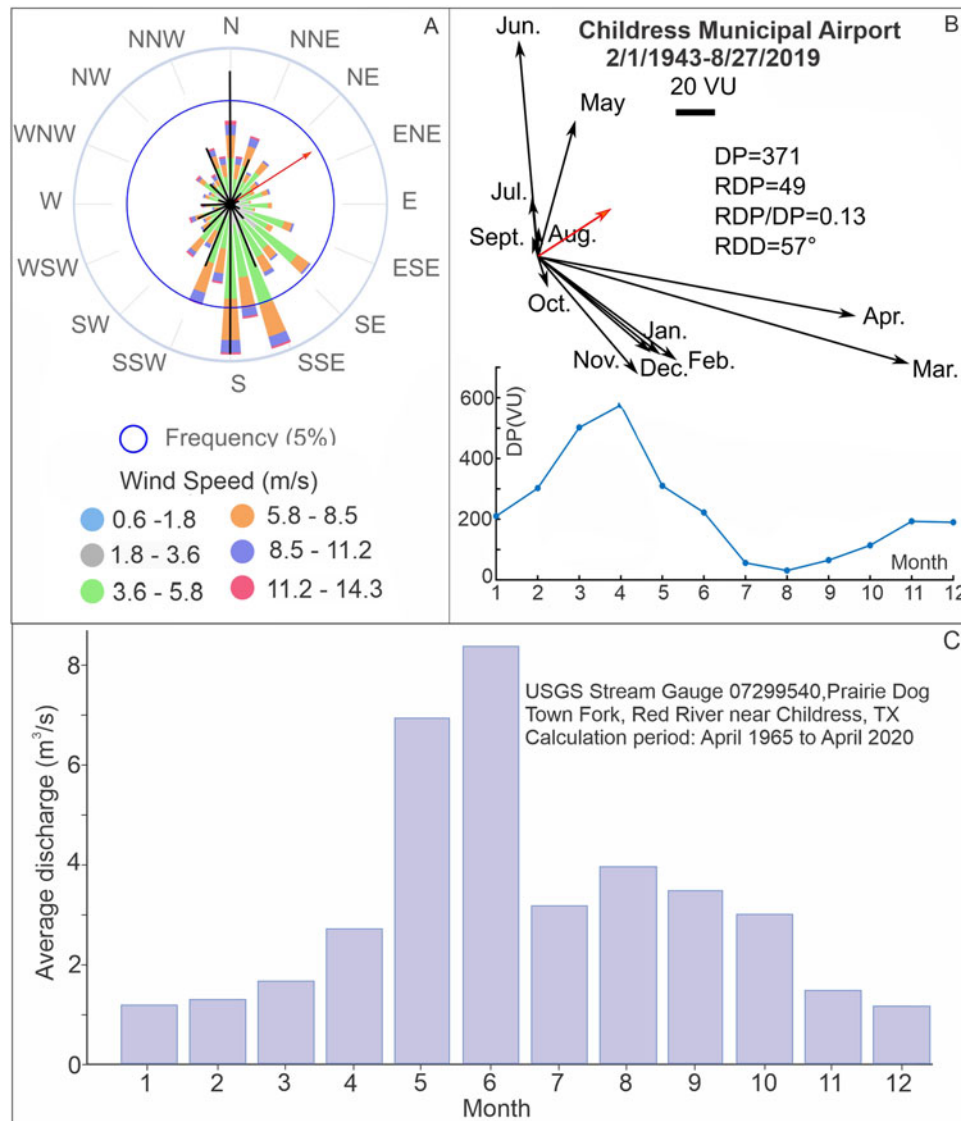


Figure 3. Wind climate for Childress Municipal Airport site with data from February 1, 1943, to August 27, 2019 (<https://www.ncdc.noaa.gov/cdo-web/datasets/GHCND/stations/GHCND:USW00023007/detail>). (A) Wind rose. (B) Wind drift potential (DP), resultant drift potential (RDP), and resultant drift direction (RDD); the lower part of B shows monthly distribution of drift potential values in vector units (VU) (Fryberger, 1979; Yizhaq et al., 2020). (C) Average monthly discharge for U.S. Geological Survey Stream Gauge 07299540 for the Prairie Dog Town Fork, Red River near Childress, TX, for the period April 1965 to April 2020 (https://water-data.usgs.gov/nwis/inventory/?site_no=07299540&agency_cd=USGS).

Municipal Airport data between 1943 and 2019 (Fig. 3A), shows significant seasonal variability (Fig. 3B). Winter and early spring wind directions are from northwest to west, with the strongest wind drift potential (Fryberger, 1979; Yizhaq et al., 2020) in March and April (Fig. 3A and B). In contrast, late spring through summer wind directions are mostly from the south, with lower wind drift potential values (Fig. 3B). Thus, the lowest discharge for the Red River (Fig. 3C), with maximum exposure of channel, bar, and floodplain surfaces, appears coincident with the highest monthly average wind drift potential for January to April (Fig. 3B), which are conditions conducive for aeolian transport from fluvial surfaces and accretion of source-border dune fields on adjacent terraces.

The western Red River is a meandering river with a broad floodplain and numerous Late Quaternary flights of geomorphologically distinct river terraces (Frye and Leonard, 1963; Edwards,

2016). These terraces were mapped by Frye and Leonard (1963) for the length of the Red River and major tributaries, and are named, from highest to lowest: Hardeman (~32 m), Ambrose (~10 m), and Cooke (~5 m). There are no direct ages for these terraces; inferred late Pleistocene ages are based on molluscan biostratigraphy and broad correlation with midwestern U.S. glacial stages such as Kansan and early and late Wisconsinan, respectively (Frye and Leonard, 1963).

In contrast, the terraces and meander belts of the lower Red River and Mississippi River valleys have been the focus of numerous studies, particularly near the confluence with the Atchafalaya River (Autin 1996; Tornqvist et al., 1996; Aslan and Autin, 1998; Shen et al., 2012). Five major fluvial allostratigraphic units—the Upland, Intermediate, Prairie, and Deweyville complexes and Holocene meander belts—have been recognized in the lower Red River and Mississippi valleys (LMV); and adjacent Gulf

Coast Plain (Blum and Valastro, 1994; Autin, 1996; Blum and Aslan, 2006; Shen et al., 2012). The Upland Complex is the oldest and highest allostratigraphic unit, with an inferred age of late Tertiary to Early Pleistocene and may preclude influences from Pleistocene glaciations (Autin, 1996). A younger allostratigraphic member is the Early to middle Pleistocene Intermediate Complex expressed in the lower Red River Valley as the Montgomery terrace, which is highly dissected (Fisk, 1938; Autin, 1996). The Prairie and Deweyville Complexes span from the late Pleistocene to the Holocene and are characterized by widespread fluvial aggradation of meandering streams (Autin, 1996). The Prairie Complex along the lower Red River deltaic plain yielded OSL ages of 91 ± 9 and 104 ± 10 ka and 111 ± 10 ka for the higher terrace at the Avoyelles Prairie site (Shen et al., 2012). In most localities in the LMV, the Prairie Complex yielded OSL ages between ca. 135 and 70 ka, a time of shoreline progradation with high and stable sea level during Marine Oxygen Isotope Stage 5 (MIS 5) (Shen et al., 2012). Two additional OSL ages of ca. 220 and 215 ka from the Prairie Complex indicate a possible earlier initiation age, during MIS 7, although this association has been questioned (Otvos, 2013). The Deweyville Complex/Formation reflects net fluvial aggradation in the middle to late Wisconsinan (Autin, 1996). A pivotal study with detailed mapping and associated OSL ages for high, well-preserved braid belts for the middle and lower LMV show fluvial aggradation ca. 64 to 11 ka in equilibrium with a steeper river gradient during the last glacial maximum (LGM) (Rittenour et al., 2007). This fluvial depositional unit is widespread along rivers and tributaries in central and southern Texas (Blum et al., 1994; Blum and Aslan, 2006), contains late Pleistocene fauna with ^{14}C ages of 26 to 20 ka old (Lundelius et al., 2013, 2019) and OSL ages between 44 and 8.6 ka (Meier et al., 2013). Studies of the Prairie and Deweyville Complexes and correlative deposits indicate that the fluvial incision in response to sea-level fall extends at least 500–600 km upstream from the current shoreline (Blum and Aslan, 2006; Rittenour et al., 2007; Shen et al. 2012). Holocene meander belts abound in the floodplain of the LMV, with a majority deposited post 5.4 ka, a period of relatively stable global sea level (Aslan and Autin, 1998). Late Holocene flood records for the middle Mississippi valley, near St. Louis, indicate periods of sustained flooding during the seventeenth and early eighteenth centuries, with anthropogenic impacts starting in nineteenth century (Munoz et al., 2015, 2018).

METHODS

Landform analysis for the upper Red River Valley

A landform analysis for the upper Red River basin was completed that shows flights of fluvial terraces often covered by aeolian sediments (Figs. 1, 2, and 4). Geomorphic mapping identified a variety of aeolian and fluvial landforms, including the active floodplain, three terraces sets at distinct heights, blowout and parabolic dunes, and sinuous ridges (Figs. 2 and 4). Surficial characteristics of landforms were revealed through analysis of multiple years of aerial photographs from the 1980s to 2020s from Google Earth Pro. Mapping was also aided by partial aerial photograph coverage from the 1930s, a time of less surface disturbance (Bolles et al., 2017), topographic maps, digital elevational models (1 and 10 m resolution), soil series maps from the Natural Resource Conservation Service, and field-based land surveys and stratigraphic studies. Mapped fluvial terraces were traced

by elevation using digital elevation models (<https://topobuilder.nationalmap.gov>; <https://www.freemaptools.com/elevation-finder.htm>) and field assessments. Many terraces were physically traced in the field (Fig. 4) and intimately associated with stratigraphic localities to better understand fluvial landform height and the nature of aeolian cover. This mapping identified three Quaternary terraces from lowest to highest—Qt1, Qt2, and Qt3—with the respective height ranges of 1 to 3, 5 to 8, and 15 to 20 m; these were assigned the respective informal names Luna, Vernon, and Childress (Figs. 1 and 2). Although, many terrace heights may be exaggerated by the later addition of meters of aeolian sediments, the Geoprobe cores used in this study provided needed data on aeolian cover thickness and age to better assess terrace elevation with respect to the current Red River level (RRL).

Sedimentary and stratigraphic analysis

The stratigraphic record of fluvial and aeolian processes and periods of landscape stability, as indicated by buried soils, was delineated through the study of four 1- to 3-m-high stratigraphic sections and six 5- to 14-m-long Geoprobe cores. Sedimentary sequences are characterized by numerous distinct depositional units of aeolian and fluvial sand, often with paleosols demarking the unit top. Usually, aeolian and fluvial stratigraphic successions represent a conservative record of depositional periods and associated hiatuses because of the unknown completeness associated with erosion and pedogenesis in terrestrial settings (e.g., Forman et al., 2022). Thus, multiple sections and sequences of cores were taken across terraces and were analyzed to capture some of the spatial and temporal variability of fluvial and aeolian processes in the late Pleistocene and Holocene for the upper Red River. Sections and Geoprobe cores were studied with attention to sedimentologic and pedogenic details, including soil structure and texture, carbonate morphologies, Munsell color changes, variability in bed thickness, nature of bed contacts, carbonate content, and the associated granulometry (Fig. 5). Attention was focused on bedding planes and unit contacts to assess whether there were hiatuses in deposition, sometimes indicated by the presence of a buried soil or localized bioturbation. The recognition of a buried soil is pivotal, because this stratigraphic marker probably reflects landscape stability associated with relatively mesic conditions. We used well-vetted soil stratigraphic and geomorphic approaches (Birkeland, 1999; Schoeneberger et al., 2012). All soil Munsell colors are assessed in the moist state. Buried soils show clear signs of rubification and secondary accumulation of clay and silt, and in places there is evidence for precipitation of pedogenic carbonate. Aeolian stratigraphic units representing discrete depositional events were defined by either bounding buried soils or sedimentologic characteristics (Fig. 5). Granulometry was determined using a Malvern Mastersizer 2000 laser diffractometer with particle size limits set by Folk (1980) to assist in determining pedosedimentary facies (Table 1).

OSL dating of aeolian and fluvial sediments

Strata were sampled for OSL dating after assessment of the pedosedimentary context (Figs. 6–8). At least one OSL sample was retrieved from each stratigraphic unit, dependent on unit thickness. Sampling in the field and laboratory avoided levels with diagenetic and pedogenetic alterations and favoring primary depositional sediments. These OSL samples were taken from stratigraphic sites using light-secure 4-cm-diameter and

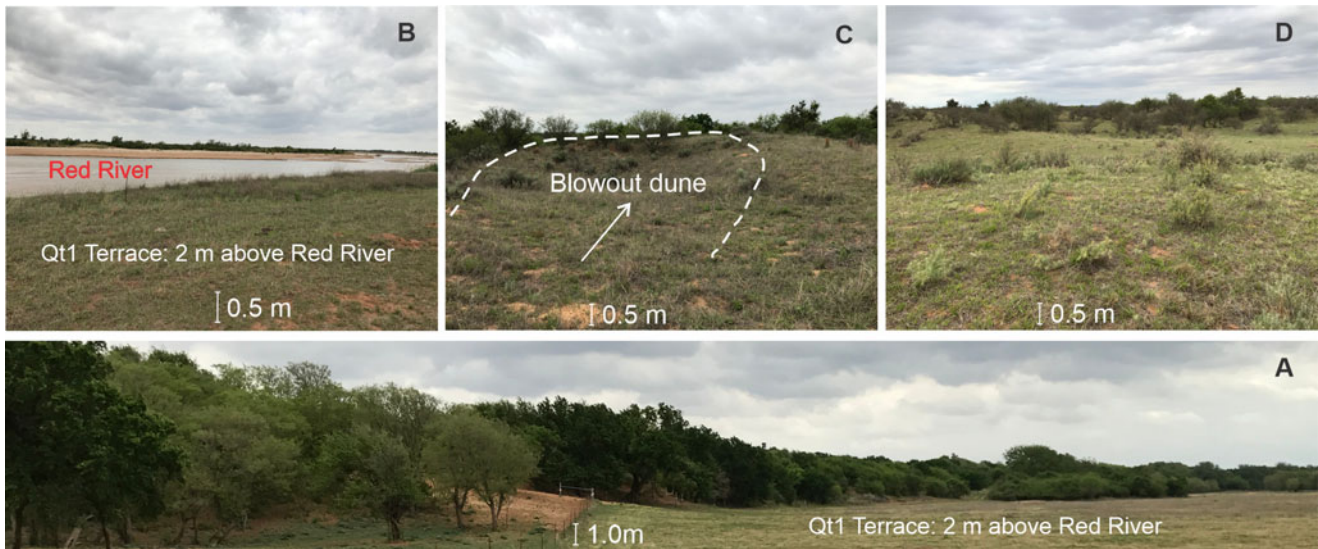


Figure 4. (A) Broad Qt1 terrace at about 2 m above Red River inset into degraded slope of Qt 2 terrace. (B) Qt1 terrace at 2 m above and incised by the Red River. (C) Blowout dune on Qt1 terrace. (D) Hummocky surface of stabilized dunes over Qt1 and Qt2 terraces.

13-cm-long sections of black ABS pipe hammered into the desired sampling level. OSL sampling for Geoprobe cores was completed under safelight conditions (Na-vapor bulb) within the Baylor Geoluminescence Dating Research Laboratory.

Single-aliquot regeneration (SAR) protocols (Murray and Wintle, 2003; Wintle and Murray, 2006) were used to estimate the equivalent dose (D_e) of quartz fractions of a certain size range for 33 to 76 separate aliquots (Table 2). Each aliquot contained ~20 to 80 quartz grains corresponding to ~1 mm circular diameter of grains adhered (with silicon) to a 0.98-cm-diameter circular aluminum disk. The separation of quartz fractions for a specific grain-size range (e.g., 63–100 μm) followed the procedure outlined in Marin *et al.* (2021). Note that all OSL ages are calculated with respect to recent corrections in beta source collaborations (Autzen *et al.*, 2022). Details of OSL dating are provided in Appendix 1 in the Supplementary Material.

RESULTS

Fluvial and aeolian depositional record of the upper Red River Valley

Three broad levels of fluvial terraces were identified immediately to about 15 to 20 m above and adjacent to the western Red River (Figs. 1, 2, and 4). These terraces occur from highest to lowest above the seasonally lowest water level (during fall and winter) as Qt3 (15–20 m), Qt2 (5–8 m), and Qt1 (1–3 m). The lowest terrace discerned was about 0.5 m above RRL, inset into the Qt1 terrace in places. Modern flood debris and abandoned channels, point bars, natural levee ridges and bars, and swale topography were common on this lowest terrace and evident on the Qt1 terrace in places, such as the Mike Site (Fig. 2A).

Aeolian deposits are common on terraces and extend the apparent height of terraces by up to 10 m in places and protect older terraces from subsequent erosion (Figs. 7 and 8). These aeolian-covered terraces were targets for extracting Geoprobe cores to discern the age and stratigraphic relation between fluvial and aeolian processes. Also, stratigraphic sections were studied along the banks of the Red River and barrow pits (Figs. 6–8).

The dune fields adjacent to the Red River are mostly stabilized and often well vegetated and occur preferentially on the inside of meander bends, where the supply of sediments may be enhanced for aeolian transport from extensive bars and wider channels (Figs. 1 and 2). Aeolian landforms are well expressed at the three study sites (Sites A, B, and C; Fig. 2), and reveal a complex diachronous relation between aeolian deposits and the underlying terraces (Figs. 7 and 8). Sites A and B show superposition relations among recent blowout dunes, older parabolic dunes, and the oldest aeolian landforms, sinuous ridges on the Qt2 and Qt3 terraces (Fig. 2). The youngest apparent landforms are blowout dunes and are well expressed riverward in stabilized dune fields at Sites A and B (Fig. 2). Blowout dunes show fresh, less-vegetated surfaces, with elongate erosion depressions of 5 to 40 m in length orientated northwest and southeast, indicating formation by winds from the west to northwest, which are dominant wind directions in the winter and early spring (Fig. 3). These blowout dunes crosscut larger and clustered parabolic dunes, which vary in length from ~50 to 200 m, often with asymmetric arms. The orientation of these parabolic dunes indicates dominant formation by winds from the west to northwest, consistent with the highest wind drift potential during March and April (Fig. 3). The apparent, oldest aeolian landform, confined to the Qt2 and Qt3 terraces, are parallel to subparallel sinuous ridges, some >1 km long. These ridges have broad crests, 10 to 30 m wide, with slope angles of 5° to 10° and no discernible consistent slope of asymmetry. The long-axis orientation of these degraded aeolian landforms is north to south, with a wind sense of formation from the west to east plane.

Pedosedimentary facies for Red River fluvial and aeolian sediments

Four pedosedimentary facies (1, 2, 3, and 4) were defined to better characterize the sedimentologic and pedogenic variability exposed in stratigraphic sections and the Geoprobe cores (Table 1). These facies are the basis for defining depositional sequences, lacunae and to infer paleoenvironments (e.g., Miall 1996; Forman *et al.*,

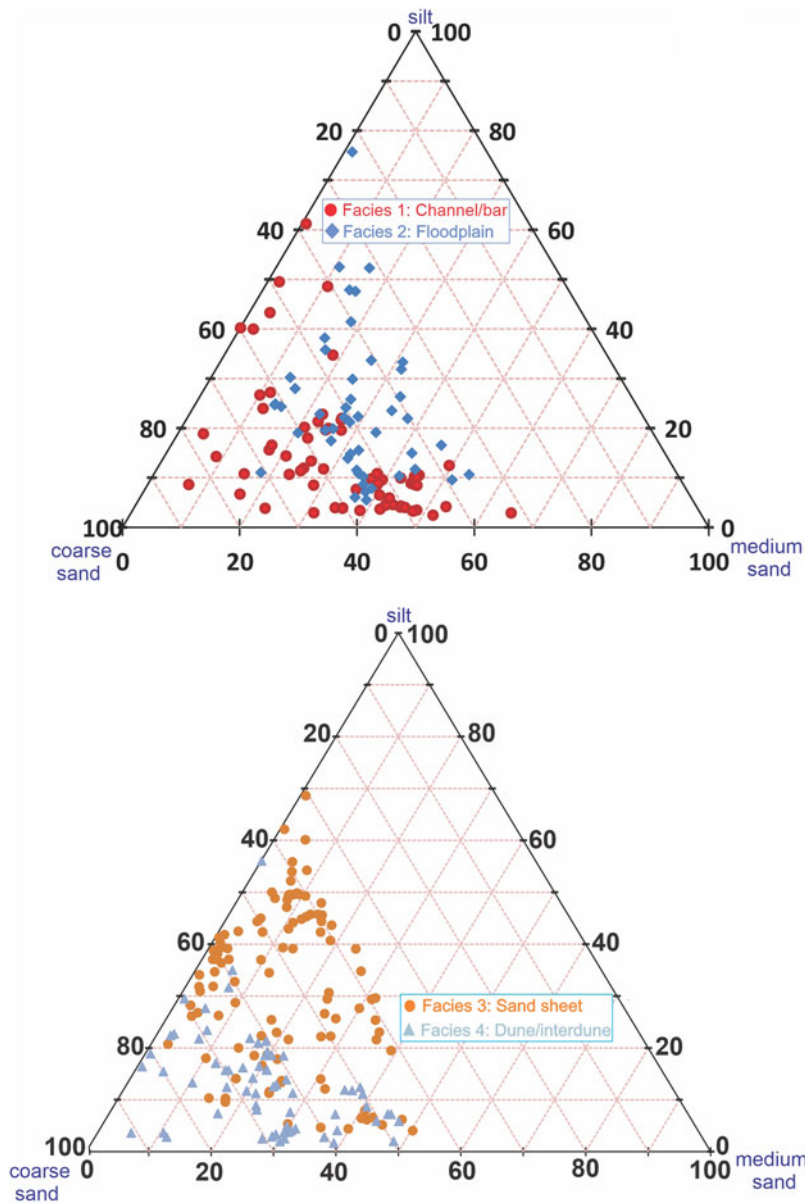






Figure 5. Ternary diagrams showing the distribution of silt and coarse and medium sand for fluvial and aeolian facies for Red River Holocene and late Pleistocene sediments.

2022). Facies are defined by the associated granulometry (Fig. 5), bedforms, contact between units, and pedogenic horizons (e.g., Bs, Bw, Bt, and Bk). Facies 1 is an orange to yellow, moderately to poorly sorted, coarse to fine sand with common small pebbles (0.5–2.0 cm in diameter), granules, and granule-size clay- and silt-rich intraclasts. This facies appears massive in cores and in places shows clear centimeter-scale bedding, with common orange to yellow iron staining. The upper boundary of this facies is often demarked by a truncated argillic or cambic horizon, reflecting subaerial exposure, landform stabilization, and subsequent erosion. These sediments are dominated by coarse sand and granules (Fig. 5), reflecting a high- to moderate-energy fluvial depositional environment associated with channel and channel margin processes. Facies 2 is finer grained than Facies 1, being a moderately well-sorted, silty to slightly silty sand (Fig. 5). It (Table 1) has a distinctive orange to yellowish-brown color with intercalated weakly to moderately developed buried soils, some with carbonate (stages 1–2), argillic and cambic morphologies.

Facies 2 is associated with low-energy fluvial environments such as floodplains or levees.

Common aeolian sediments adjacent to the Red River are represented by Facies 3 and 4. Facies 3 is a mostly massive, light yellow to gray, moderately sorted, silty fine sand to sandy silt (Fig. 5, Table 1). It is often pedogenically modified and exhibits carbonate filaments (stage 1) and weak cambic and argillic morphologies, with a well-developed buried soil demarking the upper boundary. Facies 3 can exhibit millimeter-scale subhorizontal to horizontal bedding and bedding remnants disrupted by common burrowing. It is interpreted as a sand sheet environment with intermittent deposition and pedogenesis. Facies 4, another aeolian sediment, is often coarser than Facies 3 and is composed of yellow to gray, very well sorted, medium to fine sand with less occurrence of silty sand (Fig. 5). In places it is massive, very well sorted, medium to fine sand, but can show centimeter-scale bedding in places. Facies 4 reflects interdunal and dune depositional environments, possibly associated with parabolic and barchanoid forms.

Table 1. Pedo-sedimentary facies for Red River cores showing aeolian and fluvial deposits and pedogenesis.

Pedo-sedimentary facies	Description	Depositional environment
	A well-sorted, medium to fine sand, pebbly, orange to yellowish-brown color; massive or centimeter-scale clear bedding; with Fe-staining, common soil interclast and granules, and Ab, Bw, and Bk horizons developed on the upper boundary	High-energy depositional environment associated with channel and channel marginal fluvial processes
A		
	A massive, moderately well-sorted, silty sand to slightly silty sand with granules, orange to yellowish-brown color; with carbonate filaments, may have intercalated Bk, Btk, Bt, or Bs horizons	Low-energy depositional environment associated with floodplain or levee fluvial processes
B		
	A massive, moderately well-sorted, silty sand to slightly silty sand, light yellow to gray color; with a variety of pedogenic features, carbonate filaments, with Bw, Bs, and Btk horizons intercalated or confined to the upper boundary	Pedogenically modified aeolian sand sheet
C		
	A very well sorted, fine sand, light yellow to gray color; millimeter- to centimeter-scale bedding; with modest pedogenic alterations (Ab or Bw) at the upper boundary	Dune or interdune
D		

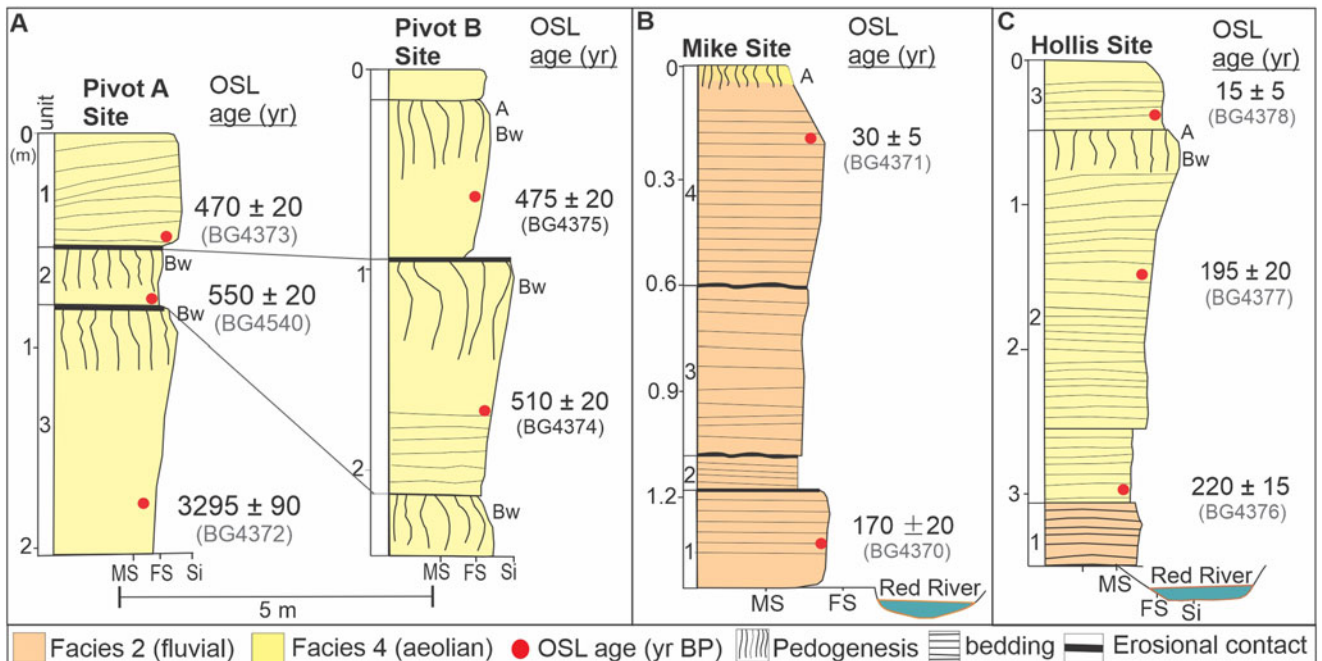


Figure 6. Stratigraphic sections (A) Pivot A and B Sites. (B) Mike Site adjacent to River Red. (C) Hollis Site showing recent aeolian deposition over fluvial sediments near river level. FS, fine sand; MS, medium sand; OSL, optically stimulated luminescence; SI, silt.

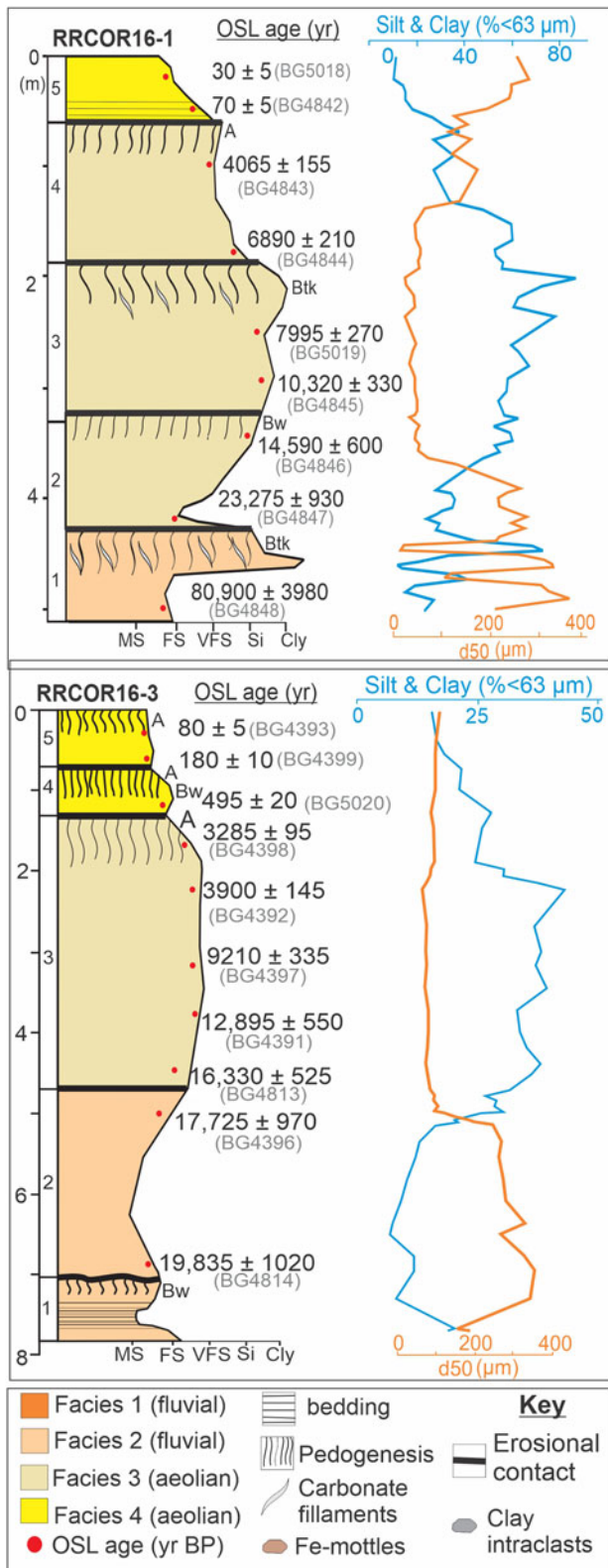


Figure 7. Stratigraphy of Geoprobe cores RRCOR16-1 and RRCOR16-3 with associated optically stimulated luminescence (OSL) ages, granulometry, and pedogenic morphologies. Particle size abbreviations: CLY, clay; FS, fine sand; MS, medium sand; Si, silt; VFS, very fine sand.

Pivot A and Pivot B Sites (34.55022°N, 100.54395°W, 573 m elevation, 21 m above the Red River)

The Pivot A and B Sites shows aeolian sediments over Qt2 or Qt3 terraces (Figs. 1 and 2A). Two sections studied in a local barrow pit, Pivot A and Pivot B, are about 10 m apart and expose the upper aeolian sand (Fig. 6). The Pivot A Site exposes the oldest stratigraphy identified, with a basal OSL age of 3295 ± 90 yr (BG4374) (Fig. 6). This basal aeolian unit (1) is massive, at least 1.2 m thick, and is composed of well-sorted, very fine to silty fine sand (Facies 3) with a cambic horizon developed in the upper 0.5 m. A similar, slightly coarser fine sand (Unit 2) unconformably overlies this lowest unit (3), with a truncate Ab at the top of Unit 2. The uppermost unit (3) is a very well sorted, fine sand with millimeter- to centimeter-scale horizontal to sub-horizontal bedding (Facies 3). Units 2 and 3 yielded the respective OSL ages of 550 ± 20 yr (BG4540) and 470 ± 20 yr (BG4373). Pivot B, a correlative section 10 m to the north of the Pivot A Site (Fig. 6), exposed the upper two units (2 and 3) with corresponding OSL ages of 475 ± 20 yr (BG4374) and 510 ± 20 yr (BG4375). These sections reflect a phase of sand sheet deposition commencing at ca. 550 to 500 yr separated by an ~50 yr period of relative landscape stability with pedogenesis forming a cambic horizon, with renewed aeolian deposition ca. 450 to 475 yr ago (Fig. 6).

Mike Site (34.5808°N, 100.5852°W, 559 m elevation, 1 m above the Red River)

The Mike Site exposes the stratigraphy at the lowest cutbank adjacent to the Red River (Fig. 6B). This site shows recent fluvial sediments, part of the floodplain, and the lowest identified tread, which forms the base of the riser for terrace Qt1 and rises 1 to 2 m above the Red River. The basal unit at this site is Facies 2-type sediment, with millimeter- to centimeter-scale horizontal beds of silty clay reflecting floodplain deposition, and yielded an OSL age of 170 ± 15 yr (BG4370). The overlying units (2 and 3) are composed of Facies 2-type sediment, fining upward from a medium to coarse sand at the base of Unit 4 to a medium to fine sand, perhaps reworked aeolian sand. OSL ages on quartz grains from the top of this section of 30 ± 5 (BG4371) indicate deposition in the late twentieth century (Fig. 6B).

Hollis Site (34.5775°N, 99.95365°W, 471 m elevation, 1.5 m above the Red River)

The Hollis Site is a section exposed along the banks of the Red River with its base at the current floodplain (Fig. 6C). This is a fining upward sequence from an overbank sediment (Facies 2) at the base capped by ~3 m of aeolian sand (Facies 3) with a clear cambic paleosol at the top of Unit 2, buried by 40 cm of recent aeolian sand (Facies 2). OSL ages on quartz grains of 220 ± 15 (BG4376) and 195 ± 20 (BG4377) from Unit 2 indicate deposition in the nineteenth century. OSL ages on the overlying aeolian sand (Unit 3) of 15 ± 5 (BG4378) demonstrate recent deposition in the past decade from the adjacent Red River floodplain (Fig. 6C).

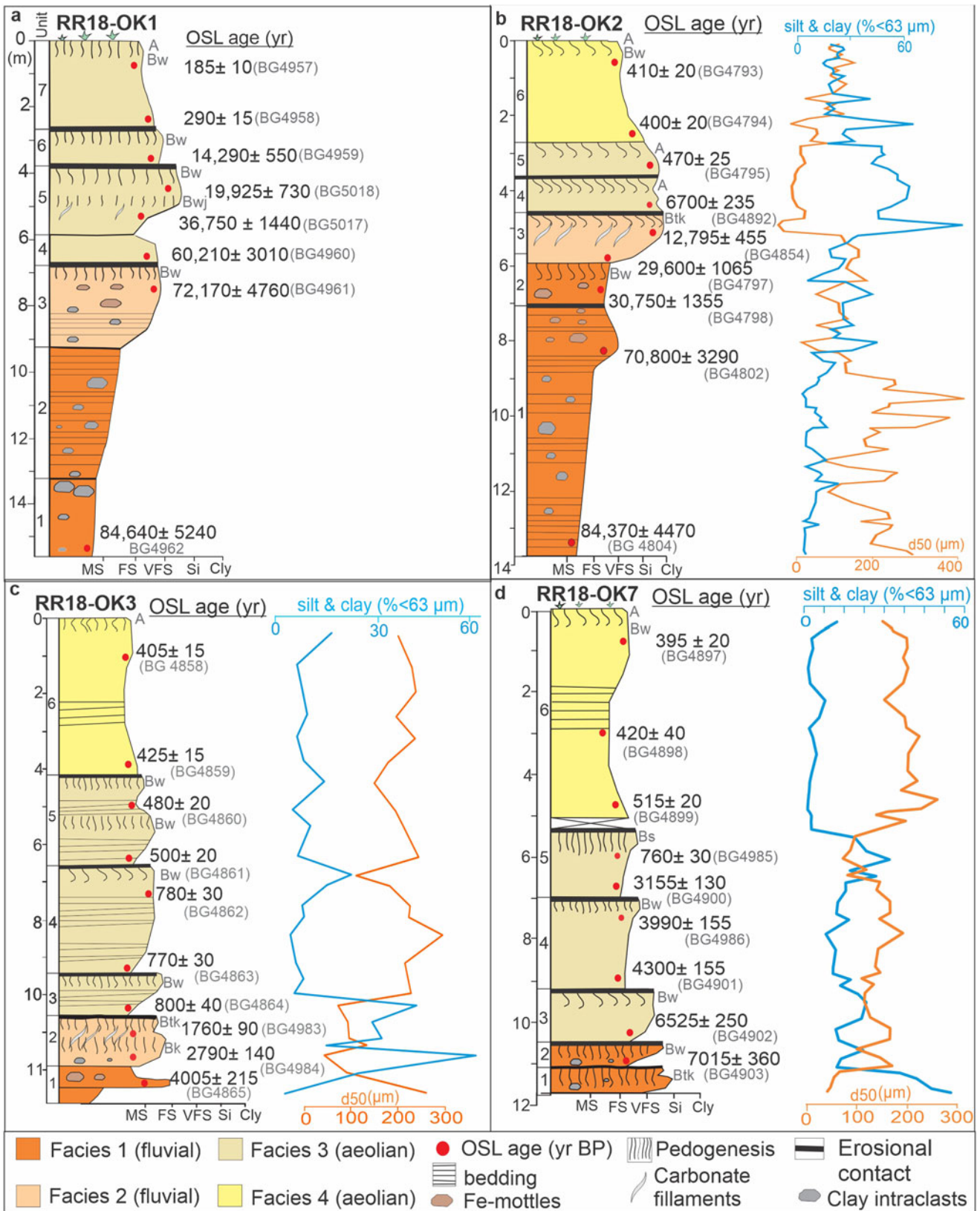


Figure 8. Stratigraphy of Geoprobe cores RR18-OK1, OK2, OK3, and OK7 with associated optically stimulated luminescence (OSL) ages, granulometry, and pedogenic morphologies. Particle size abbreviations: CLY, clay; FS, fine sand; MS, medium sand; SI, silt; VFS, very fine sand. <math>$63 \mu\text{m}$).>

Table 2. Optically stimulated luminescence (OSL) ages on quartz grain extracts and associated data for aeolian and fluvial sediments from Red River study area, Texas and Oklahoma.

Sample no./ depth (m)	Lab no.	Grain size		D_e (Gray) ^b	OD (%) ^c	U (ppm) ^d	Th (ppm) ^d	K (ppm) ^d	Rb (ppm) ^d	(%)	Cosmic dose (mGray/yr) ^e	Dose rate (mGray/yr)	OSL age (yr) ^f
		Aliquots ^a	(μ m)										
RR16-02/0.25	BG4371	63/68	150–250	0.06 ± 0.01	85 ± 8	0.76 ± 0.01	2.45 ± 0.01	0.87 ± 0.01	31.3 ± 0.1	5 ± 2	0.26 ± 0.02	1.60 ± 0.04	30 ± 5
RR16-01/1.30	BG4370	50/59	150–250	0.27 ± 0.02	51 ± 5	0.75 ± 0.01	2.50 ± 0.01	1.12 ± 0.01	39.9 ± 0.01	7 ± 2	0.20 ± 0.02	1.54 ± 0.03	170 ± 20
RR16-05/0.50	BG4373	32/35	100–150	0.81 ± 0.02	15 ± 2	0.98 ± 0.01	3.22 ± 0.01	1.07 ± 0.01	38.3 ± 0.1	3 ± 1	0.24 ± 0.02	1.66 ± 0.03	470 ± 20
RR16-04/0.80	BG4540	31/35	150–250	1.10 ± 0.03	14 ± 2	1.48 ± 0.01	3.46 ± 0.01	1.26 ± 0.01	43.5 ± 0.01	5 ± 2	0.21 ± 0.02	1.93 ± 0.05	550 ± 20
RR16-03/1.85	BG4372	33/34	100–150	6.91 ± 0.11	8 ± 1	1.48 ± 0.01	4.46 ± 0.01	1.38 ± 0.01	47.5 ± 0.01	7 ± 2	0.17 ± 0.02	1.87 ± 0.05	3295 ± 90
RR16-07/0.75	BG4375	46/50	100–150	0.80 ± 0.03	18 ± 2	1.17 ± 0.01	3.13 ± 0.01	1.04 ± 0.01	36.6 ± 0.1	5 ± 2	0.22 ± 0.02	1.65 ± 0.04	475 ± 20
RR16-06/1.65	BG4374	41/45	100–150	0.90 ± 0.02	11 ± 1	1.23 ± 0.01	3.46 ± 0.01	1.10 ± 0.01	38.9 ± 0.01	5 ± 2	0.19 ± 0.02	1.76 ± 0.04	510 ± 20
RR16-12/0.40	BG4378	42/48	150–250	0.03 ± 0.004	92 ± 10	0.78 ± 0.01	2.21 ± 0.01	0.82 ± 0.01	35.0 ± 0.01	15 ± 3	0.25 ± 0.02	1.36 ± 0.04	15 ± 5
RR16-10/1.50	BG4377	41/43	150–250	0.20 ± 0.02	36 ± 4	0.64 ± 0.01	2.15 ± 0.01	0.95 ± 0.01	31.6 ± 0.01	20 ± 5	0.19 ± 0.02	1.19 ± 0.05	195 ± 20
RR16-09/3.00	BG4376	33/34	150–250	0.26 ± 0.01	22 ± 3	0.64 ± 0.01	1.85 ± 0.01	1.04 ± 0.01	35.0 ± 0.01	30 ± 5	0.16 ± 0.02	1.12 ± 0.05	220 ± 15
RR18-OK1A/0.4	BG4957	38/48	150–250	0.31 ± 0.01	17 ± 4	0.57 ± 0.01	1.87 ± 0.01	1.17 ± 0.01	41.1 ± 0.01	5 ± 2	0.23 ± 0.02	1.57 ± 0.04	185 ± 10
RR18-OK1B/2.6	BG4958	36/39	150–250	0.41 ± 0.02	22 ± 3	0.52 ± 0.01	1.57 ± 0.01	1.03 ± 0.01	35.8 ± 0.01	5 ± 2	0.17 ± 0.02	1.34 ± 0.03	290 ± 15
RR18-OK1C/3.6	BG4959	34/40	100–150	28.28 ± 0.90	17 ± 2	1.17 ± 0.01	4.09 ± 0.01	1.68 ± 0.01	50.7 ± 0.01	7 ± 2	0.15 ± 0.02	1.98 ± 0.05	14,290 ± 550
RR18-OK1D/4.3	BG5016	39/40	150–250	34.55 ± 1.02	22 ± 3	1.14 ± 0.01	3.68 ± 0.01	1.28 ± 0.01	48.2 ± 0.01	10 ± 2	0.14 ± 0.01	1.73 ± 0.04	19,925 ± 730
RR18-OK1E/5.4	BG5017	47/50	150–250	50.23 ± 1.24	16 ± 2	0.97 ± 0.01	1.66 ± 0.01	1.14 ± 0.01	41.1 ± 0.01	15 ± 3	0.12 ± 0.01	1.37 ± 0.04	36,750 ± 1440
RR18-OK1F/6.6	BG4960	33/40	150–250	84.21 ± 3.264	20 ± 3	0.72 ± 0.01	2.34 ± 0.01	1.12 ± 0.01	41.4 ± 0.01	15 ± 3	0.11 ± 0.01	1.40 ± 0.04	60,210 ± 3010
RR18-OK1F/7.3	BG4961	32/40	150–250	145.80 ± 8.32	22 ± 3	1.47 ± 0.01	4.95 ± 0.01	1.54 ± 0.01	56.8 ± 0.01	15 ± 3	0.11 ± 0.01	2.02 ± 0.04	72,170 ± 4760
RR18-OK1F/15	BG4962	32/39	250–355	84.40 ± 3.68	22 ± 3	0.52 ± 0.01	1.28 ± 0.01	0.99 ± 0.01	31.1 ± 0.01	20 ± 5	0.06 ± 0.01	0.98 ± 0.05	84,640 ± 5240
RR18-OK2A/0.6	BG4793	42/48	150–250	0.70 ± 0.02	20 ± 2	0.66 ± 0.01	1.93 ± 0.01	1.27 ± 0.01	39.8 ± 0.01	5 ± 2	0.22 ± 0.02	1.68 ± 0.04	410 ± 20
RR18-OK2C/3.0	BG4794	43/48	100–150	0.97 ± 0.04	23 ± 3	2.14 ± 0.01	6.44 ± 0.01	1.42 ± 0.01	54.4 ± 0.01	7 ± 2	0.16 ± 0.02	2.38 ± 0.05	400 ± 20
RR18-OK2C/3.3	BG4795	72/76	63–100	1.29 ± 0.06	46 ± 5	2.32 ± 0.01	6.26 ± 0.01	1.70 ± 0.01	55.4 ± 0.01	7 ± 2	0.15 ± 0.02	2.68 ± 0.08	470 ± 25
RR18-OK2D/4.40	BG4982	38/40	100–150	18.40 ± 0.63	21 ± 2	1.96 ± 0.01	7.12 ± 0.01	1.74 ± 0.01	55.8 ± 0.01	10 ± 2	0.14 ± 0.01	2.59 ± 0.06	6700 ± 235
RR18-OK2D/4.66	BG4854	35/35	100–150	27.06 ± 0.77	16 ± 2	1.62 ± 0.01	5.54 ± 0.01	1.42 ± 0.01	48.4 ± 0.01	10 ± 2	0.13 ± 0.01	2.11 ± 0.05	12,795 ± 455
RR18-OK2D/4.87	BG4796	35/35	150–250	28.83 ± 1.00	21 ± 2	1.66 ± 0.01	5.30 ± 0.01	1.51 ± 0.01	51.9 ± 0.01	10 ± 2	0.13 ± 0.01	2.14 ± 0.05	13,465 ± 545
RR18-OK2E/5.90	BG4797	46/48	150–250	50.04 ± 1.40	16 ± 2	1.56 ± 0.01	2.43 ± 0.01	1.24 ± 0.01	39.2 ± 0.01	10 ± 2	0.12 ± 0.01	1.69 ± 0.04	29,600 ± 1065
RR18-OK2E/6.30	BG4798	43/48	150–250	50.82 ± 1.83	21 ± 2	0.74 ± 0.01	2.19 ± 0.01	1.42 ± 0.01	46.7 ± 0.01	10 ± 2	0.11 ± 0.01	1.65 ± 0.05	30,750 ± 1355
RR18-OK2G/8.60	BG4802	28/34	150–250	123.67 ± 4.25	16 ± 3	1.21 ± 0.01	3.69 ± 0.01	1.85 ± 0.01	48.5 ± 0.01	20 ± 4	0.09 ± 0.01	1.75 ± 0.07	70,800 ± 3290
RR18-OK2K/14.20	BG4804	37/40	250–355	95.83 ± 3.62	20 ± 3	0.73 ± 0.01	1.86 ± 0.01	1.10 ± 0.01	32.6 ± 0.01	20 ± 4	0.06 ± 0.01	1.14 ± 0.05	84,640 ± 4470
RR18-OK3A/1.03	BG4858	45/48	150–250	0.61 ± 0.01	11 ± 2	0.63 ± 0.01	2.03 ± 0.01	1.08 ± 0.01	32.3 ± 0.01	5 ± 2	0.20 ± 0.02	1.47 ± 0.04	405 ± 15
RR18-OK3D/3.97	BG4859	45/48	150–250	0.52 ± 0.01	12 ± 2	0.75 ± 0.01	1.32 ± 0.01	0.92 ± 0.01	29.5 ± 0.01	10 ± 2	0.14 ± 0.01	1.19 ± 0.03	425 ± 15

(Continued)

Table 2. (Continued.)

Sample no./ depth (m)	Lab no.	Grain size		D_e (Gray) ^b	OD (%) ^c	U (ppm) ^d	Th (ppm) ^d	K (ppm) ^d	Rb (ppm) ^d	(%)	Cosmic dose (mGray/yr) ^e	Dose rate (mGray/yr)	OSL age (yr) ^f
		Aliquots ^a	(μ m)										
RR18-OK3E/4.96	BG4860	48/48	150–250	0.65 ± 0.02	14 ± 2	0.58 ± 0.01	1.81 ± 0.01	1.09 ± 0.01	35.2 ± 0.01	10 ± 2	0.12 ± 0.01	1.31 ± 0.03	480 ± 20
RR18-OK3F/6.57	BG4861	46/48	150–250	0.64 ± 0.02	13 ± 2	0.44 ± 0.01	1.35 ± 0.01	1.10 ± 0.01	35.3 ± 0.01	10 ± 2	0.11 ± 0.01	1.26 ± 0.03	500 ± 20
RR18-OK3F/7.32	BG4862	46/48	150–250	1.13 ± 0.04	11 ± 2	0.65 ± 0.01	1.83 ± 0.01	1.23 ± 0.01	36.7 ± 0.01	10 ± 2	0.10 ± 0.01	1.42 ± 0.03	780 ± 30
RR18-OK3H/9.33	BG4863	45/54	150–250	0.96 ± 0.01	22 ± 3	0.63 ± 0.01	2.00 ± 0.01	1.09 ± 0.01	34.9 ± 0.01	15 ± 3	0.08 ± 0.01	1.23 ± 0.04	770 ± 30
RR18-OK3I/10.46	BG4864	42/49	150–250	0.94 ± 0.01	23 ± 3	0.63 ± 0.01	1.75 ± 0.01	1.10 ± 0.01	33.9 ± 0.01	20 ± 5	0.07 ± 0.01	1.17 ± 0.05	800 ± 40
RR18-OK3I/11.00	BG4983	40/40	100–150	3.26 ± 0.07	11 ± 1	1.39 ± 0.01	4.30 ± 0.01	1.54 ± 0.01	49.5 ± 0.01	20 ± 5	0.08 ± 0.01	1.85 ± 0.08	1760 ± 90
RR18-OK3I/11.60	BG4984	39/39	150–250	4.21 ± 0.10	10 ± 1	0.96 ± 0.01	2.64 ± 0.01	1.39 ± 0.01	42.5 ± 0.01	20 ± 5	0.07 ± 0.01	1.50 ± 0.07	2790 ± 140
RR18-OK3J/12.60	BG4865	47/48	63–100	8.89 ± 0.22	16 ± 2	1.61 ± 0.01	4.63 ± 0.01	1.90 ± 0.01	59.3 ± 0.01	20 ± 5	0.06 ± 0.01	2.21 ± 0.11	4005 ± 215
RR18-OK7A/0.85	BG4897	39/40	150–250	0.61 ± 0.02	16 ± 2	0.66 ± 0.01	2.11 ± 0.01	1.18 ± 0.01	40.7 ± 0.01	5 ± 2	0.20 ± 0.02	1.51 ± 0.04	395 ± 20
RR18-OK7C/3.00	BG4998	34/40	250–355	0.64 ± 0.06	31 ± 4	0.71 ± 0.01	2.02 ± 0.01	1.45 ± 0.01	42.1 ± 0.01	7 ± 2	0.16 ± 0.02	1.50 ± 0.04	420 ± 40
RR18-OK7D/4.81	BG4899	37/40	100–150	0.86 ± 0.02	12 ± 2	0.75 ± 0.01	2.05 ± 0.01	1.35 ± 0.01	44.5 ± 0.01	10 ± 2	0.13 ± 0.01	1.64 ± 0.04	515 ± 20
RR18-OK7E/6.00	BG4985	39/39	100–150	1.59 ± 0.04	13 ± 2	1.62 ± 0.01	5.35 ± 0.01	1.52 ± 0.01	49.2 ± 0.01	15 ± 3	0.12 ± 0.01	2.07 ± 0.06	760 ± 30
RR18-OK7F/6.85	BG4900	38/40	150–250	5.10 ± 0.13	12 ± 2	1.06 ± 0.01	3.18 ± 0.01	1.32 ± 0.01	44.0 ± 0.01	15 ± 3	0.11 ± 0.01	1.61 ± 0.05	3155 ± 130
RR18-OK7F/7.40	BG4986	39/40	150–250	5.56 ± 0.08	7 ± 1	0.76 ± 0.01	2.34 ± 0.01	1.44 ± 0.01	40.3 ± 0.01	15 ± 3	0.10 ± 0.01	1.39 ± 0.04	3990 ± 135
RR18-OK7G/8.96	BG4901	40/40	100–150	7.06 ± 0.11	7 ± 1	1.15 ± 0.01	2.72 ± 0.01	1.62 ± 0.01	42.8 ± 0.01	15 ± 3	0.09 ± 0.01	1.64 ± 0.05	4300 ± 155
RR18-OK7H/10.29	BG4902	35/40	150–250	9.26 ± 0.16	4 ± 2	0.85 ± 0.01	2.11 ± 0.01	1.24 ± 0.01	38.7 ± 0.01	15 ± 3	0.08 ± 0.01	1.42 ± 0.04	6525 ± 250
RR18-OK7I/10.95	BG4903	38/40	150–250	9.56 ± 0.22	8 ± 2	0.95 ± 0.01	2.32 ± 0.01	1.23 ± 0.01	40.2 ± 0.01	20 ± 5	0.08 ± 0.01	1.36 ± 0.06	7015 ± 360
RR16-1A/0.30	BG5018	37/50	250–355	0.06 ± 0.005	72 ± 4	0.88 ± 0.01	3.20 ± 0.01	1.00 ± 0.01	35.0 ± 0.01	5 ± 2	0.25 ± 0.02	1.54 ± 0.02	30 ± 5
RR16-1A/0.54	BG4842	53/73	150–250	0.14 ± 0.01	89 ± 9	1.03 ± 0.01	3.43 ± 0.01	1.36 ± 0.01	35.6 ± 0.01	5 ± 2	0.24 ± 0.02	1.74 ± 0.02	70 ± 5
RR16-1A/1.1	BG4843	38/40	150–250	8.44 ± 0.20	13 ± 2	1.47 ± 0.01	4.46 ± 0.01	1.34 ± 0.01	44.8 ± 0.01	5 ± 2	0.20 ± 0.02	2.07 ± 0.05	4065 ± 155
RR16-1B/1.9	BG4844	40/40	63–100	19.79 ± 0.40	9 ± 1	2.01 ± 0.01	7.30 ± 0.01	1.78 ± 0.01	58.8 ± 0.01	5 ± 2	0.18 ± 0.02	2.86 ± 0.06	6890 ± 210
RR16-1C/2.4	BG5019	40/40	150–250	20.56 ± 0.53	15 ± 2	1.99 ± 0.01	7.07 ± 0.01	1.74 ± 0.01	63.4 ± 0.01	10 ± 2	0.17 ± 0.02	2.57 ± 0.06	7995 ± 270
RR16-1C/2.9	BG4845	38/40	63–100	26.53 ± 0.53	9 ± 1	1.98 ± 0.01	7.41 ± 0.01	1.64 ± 0.01	56.8 ± 0.01	10 ± 2	0.17 ± 0.02	2.57 ± 0.06	10,320 ± 300
RR16-1C/3.4	BG4846	38/40	150–250	31.28 ± 1.03	18 ± 2	1.55 ± 0.01	5.77 ± 0.01	1.48 ± 0.01	52.3 ± 0.01	10 ± 2	0.16 ± 0.02	2.14 ± 0.05	14,590 ± 600
RR16-1D/4.1	BG4847	37/40	150–250	38.27 ± 1.27	18 ± 2	1.03 ± 0.01	3.43 ± 0.01	1.21 ± 0.01	39.6 ± 0.01	10 ± 2	0.15 ± 0.02	1.64 ± 0.04	23,275 ± 930
RR16-1D/4.9	BG4848	36/39	150–250	102.16 ± 3.99	21 ± 3	0.76 ± 0.01	2.10 ± 0.01	1.02 ± 0.01	33.3 ± 0.01	15 ± 3	0.14 ± 0.01	1.26 ± 0.04	80,900 ± 3980
RR16-3/0.33	BG4393	27/33	63–100	0.20 ± 0.01	36 ± 5	1.86 ± 0.01	5.12 ± 0.01	1.23 ± 0.01	50.3 ± 0.01	5 ± 2	0.25 ± 0.02	2.10 ± 0.05	80 ± 5
RR16-3/0.65	BG4399	27/33	63–100	0.40 ± 0.01	36 ± 5	1.86 ± 0.01	5.12 ± 0.01	1.23 ± 0.01	50.3 ± 0.01	10 ± 2	0.22 ± 0.02	2.29 ± 0.05	180 ± 10
RR16-3/1.20	BG5020	42/44	100–150	1.19 ± 0.04	19 ± 2	2.17 ± 0.01	5.69 ± 0.01	1.45 ± 0.01	47.4 ± 0.01	10 ± 2	0.20 ± 0.02	2.34 ± 0.06	495 ± 20
RR16-3/1.65	BG4398	35/35	150–250	7.54 ± 0.14	10 ± 1	2.18 ± 0.01	5.99 ± 0.01	1.33 ± 0.01	52.9 ± 0.01	10 ± 2	0.17 ± 0.02	2.29 ± 0.04	3285 ± 95

(Continued)

Table 2. (Continued.)

Sample no./ depth (m)	Grain size		D _e (Gray) ^b	OD (%) ^c	U (ppm) ^d	Th (ppm) ^d	K (ppm) ^d	Rb (ppm) ^d	Cosmic dose (mGray/yr) ^e	Dose rate (mGray/yr)	OSL age (yr) ^f		
	Aliquots ^a	(μm)											
RR16-3/2.00	BG4392	34/35	63-100	8.62 ± 0.16	10 ± 1	2.13 ± 0.01	6.44 ± 0.01	1.27 ± 0.01	50.7 ± 0.01	10 ± 2	0.17 ± 0.02	2.20 ± 0.06	3900 ± 145
RR16-3/3.30	BG4397	35/35	150-250	17.90 ± 0.50	16 ± 2	1.63 ± 0.01	4.87 ± 0.01	1.30 ± 0.01	44.1 ± 0.01	10 ± 2	0.16 ± 0.02	1.95 ± 0.06	9210 ± 335
RR16-3/3.60	BG4391	35/35	150-250	18.13 ± 0.51	16 ± 2	1.05 ± 0.01	3.12 ± 0.01	0.95 ± 0.01	33.5 ± 0.01	10 ± 2	0.15 ± 0.02	1.40 ± 0.03	12,895 ± 550
RR16-3/4.33	BG4813	45/45	150-250	21.70 ± 0.46	13 ± 1	0.83 ± 0.01	2.32 ± 0.01	1.01 ± 0.01	30.1 ± 0.01	15 ± 3	0.12 ± 0.01	1.33 ± 0.03	16,330 ± 525
RR16-3/5.00	BG4396	35/35	255-355	19.15 ± 0.53	15 ± 2	0.64 ± 0.01	1.79 ± 0.01	0.90 ± 0.01	32.8 ± 0.01	15 ± 3	0.13 ± 0.01	1.08 ± 0.03	17,725 ± 970
RR16-3/6.86	BG4814	40/40	150-250	21.00 ± 0.51	14 ± 2	0.70 ± 0.01	2.04 ± 0.01	0.88 ± 0.01	31.3 ± 0.1	20 ± 5	0.11 ± 0.01	1.06 ± 0.05	19,835 ± 1020

^aAliquot number used for single-aliquot regeneration (SAR). Equivalent dose calculated using the central age model of Galbraith and Roberts (2012).
^bD_e (equivalent dose) calculated on a pure quartz fraction with about 40–100 grains/aliquot and analyzed under blue-light excitation (470 ± 20 nm) by SAR protocols (Murray and Wintle, 2003; Wintle and Murray, 2006). The central age model of Galbraith et al. (1999) was used to calculate D_e when overdispersion (OD) values are <20%. The minimum age model was used with OD values >20% to resolve the youngest D_e population.
^cOD values reflect precision beyond instrumental errors; OD values of ≤20 indicate low dispersion in D_e values with a lognormal distribution (Galbraith and Roberts, 2012).
^dU, Th, Rb, and K₂O content analyzed by inductively coupled plasma-mass spectrometry (ICP-MS) analyzed by ALS Minerals Incorporation, Reno, NV, USA.
^eFrom Prescott and Hutton (1994) and Liang and Forman (2019).
^fSystematic and random errors calculated in a quadrature at 1 SD. Datum year is AD 2010. Age computation through the Luminescence Dose and Age Calculator (LDAC) at: <https://www.baylor.edu/geosciences/index.php?id=962356> (Liang and Forman, 2019).

Core RRCOR16-1 (34.54944°N, 100.0081°W, 487 m elevation, 11.5 m above the Red River)

Core RRCOR16-1 was taken from terrace 2 surface covered by Pleistocene/Holocene aeolian deposits (Figs. 1 and 4). This core contains over 4 m of aeolian sediment, mostly of Facies 3, spanning from ca. 23.3 ka to 30 yr ago (Fig. 7, Table 2). These aeolian sands bury an argillic and carbonate-rich soil, developed in fluvial deposits (Facies 2), that yielded an OSL age of 80,900 ± 3980 yr (BG4848). This oldest aeolian sediment (Unit 2) is a moderately well-sorted, medium sand that fines upward to a sandy silt, transitioning to a truncated Bw horizon developed at the unit top. This cover sand was deposited between ca. 23 and 14 ka. Unconformably overlying Unit 2 is a finer, cover loam aeolian sediment (Unit 3) with >60% silt and clay that yielded OSL ages between ca. 10 and 8 ka (Fig. 7). Aeolian sedimentation in Unit 4 renewed ca. 6.9 ka with emplacement of a moderately sorted, silty sand until ca. 4 ka, transitioning to a cummulic buried A horizon that marks the top of Unit 4. The uppermost aeolian, Unit 5, is 0.5-m-thick, moderately well-sorted, fine to medium sand to silty-fine sand with affinities to Facies 4. Quartz grains from the base of Unit 5, 40 cm below the current surface, returned an OSL age of 70 ± 5 yr (BG4842), and grains 15 cm below the surface gave an OSL age of 30 ± 5 yr (BG5018) indicating recent reworking of sediments.

RRCOR16-3 (34.56222°N, 99.94806°W, 491 m elevation, 23 m above the Red River)

Core RRCOR16-3 was taken on the downwind edge of mapped Holocene aeolian deposits, which appears to be a stabilized, vegetated paleo-dune field that buried the Qt2 or Qt3 terrace (Figs. 2 and 7). The basal sediments (Units 1 and 2) of this core from 7.9 to 4.7 m deep revealed a distinct reddish-yellow, moderately to poorly sorted, medium to coarse, granular-rich subrounded sand with rare small, rounded pebbles, characteristic of fluvial Facies 1 (Fig. 7). Quartz grains from unit 2 near the base of this core yielded an OSL age of 19,835 ± 1020 yr (BG4814), and grains 15 cm below the top of Unit 2 returned an age of 17,725 ± 970 (BG4390). Unconformably overlying Unit 2 is a massive, finer sediment, sandy silt to silty sand (Unit 3), with a paleosol demarcating the upper boundary. A stratigraphic sequence of six OSL ages from Unit 3 indicates conformable sand sheet deposition (Facies 3) between ca. 13.0 and 3.3 ka, with the upper boundary between Units 3 and 4 at a truncated buried A horizon. The two uppermost Units, 4 and 5, are sandier than subjacent sediments (Facies 4), separated by an A horizon that spans ca. 500 yr (Fig. 7).

Core RR18-OK1 (34.22833°N 99.09911°W, 356 m elevation, 13.0 m above the Red River)

Core RR18-OK1 was taken within a stabilized dune field at a prominent meander bend in the Red River with a broad floodplain (Fig. 4C). This core revealed >7 m thickness (Units 1–3) of a fining upward sequence of fluvial sediments (Facies 1 and 2) with bounding ages of ca. 84.6 and 72.2 ka (Fig. 8A). Overlying these fluvial sediments are four separate aeolian sand units (Units 4–7; Fig. 8A). The lowest aeolian unit (4) is a moderately sorted, massive, silty sand that yielded an OSL age of 60,210 ± 3010 yr (BG4960). The overlying Unit 5 is a moderately well-sorted, medium to fine sand, with the upper ~1 m showing

two compound, buried Bw horizons. Quartz grains from Unit 6, defined by bounding paleosols (Fig. 8A), returned an OSL age of $14,290 \pm 730$ yr (BG4959). The uppermost 2.7 m that defines the surface dunes (Unit 7) was a moderately well-sorted, medium to fine sand that gave the bounding OSL ages of 290 ± 15 yr (BG4958) and 185 ± 10 yr (BG4957) (Fig. 8A).

Core RR18-OK2 (34.240706°N, 99.1159436°W, 361 m elevation, 18.0 m above the Red River)

Core RR18-OK2 was taken about 2 km southwest of RR18-OK1 at the northern margin of the mapped paleo-dune field (Fig. 2C). This core revealed over 9 m of a fining upward sequence of fluvial sediment (Facies 1 and 2) succeeded by over 4 m of aeolian sand with two intercalated buried soils (Fig. 8B). The lowermost unit (1) is a high-energy fluvial facies (1) with abundant clay-rich intraclasts, granules, and common small, rounded pebbles. Quartz grains from the base and the top of the lowest unit (1) returned OSL ages of $84,640 \pm 4470$ yr (BG4804) and $70,800 \pm 3290$ yr (BG4802), respectively, and appear correlative with Units 1–3 of core RR18-OK1 (Fig. 7). In contrast, core RR18-OK2 has overlying younger fluvial sediments, Units 2 and 3, with respective OSL ages of 30.8 ka and 29.6 to 12.8 ka (Fig. 8B). Fluvial sediments of Unit 3 are bounded by two prominent paleosols. The overlying moderately sorted, sandy silt (Unit 4) is a cover sand-like deposit laid down ca. 6.7 ka. The top of Unit 4 is designated by a truncated cambic horizon, buried by a moderately sorted, silty fine sand, similar to subjacent Unit 3, that returned an OSL age of 470 ± 25 yr (BG4795). The uppermost aeolian silty sand (Unit 6), nearly 3 m thick, yielded the corresponding bottom and top OSL ages of 400 ± 20 yr (BG4794) and 410 ± 20 yr (BG4793).

Core RR18-OK3 (34.22237°N, 99.09833°W, 352 m elevation, 9.0 m above the Red River)

Core RR18-OK3 was taken at the riverward edge of the stabilized dune field, closest to a possible fluvial sediment source for adjacent dunes (Fig. 2C). This core showed 10.5 m of aeolian sands over 1.5 m of fluvial sediment (Fig. 8C). The lowest fluvial sediment (Unit 1) is characteristic of Facies 1, with a coarsening upward sequence with common silty-clay intraclasts. Quartz grains from a fine sand lens returned an OSL age of 4005 ± 215 yr (BG4865). The overlying Unit 2 is a finer-grained overbank deposit (Facies 2) with compound argillic and carbonate (stage 1) buried soil horizons. OSL ages of 2790 ± 140 yr (BG4884) and 1760 ± 90 yr (BG4983) from the base and top of Unit 2 constrain timing of aggradation. Thus, fluvial aggregation commenced at least 4.0 ka and stabilized at ca. 1.6 ka, as indicated by buried soils (in Unit 2), at about 1 to 2 m above the present RRL (Fig. 8C).

Unconformably above the basal fluvial sediments are multiple, Facies 3-type sediments of a sand sheet, Units 3–6. These units are characterized by individual fining upward sequences from a slightly silty sand to sandy silt, reflecting stabilization with the occurrence of truncated buried soil at the upper boundary of units (Fig. 8C). Five OSL ages from the base of Units 3–5 indicate that these sand sheet sediments, separated by cambic buried soil horizons were deposited during three depositional phases at ca. 780 to 750 yr, 500 to 450 yr, and 425 to 400 yr (Fig. 8C). The uppermost, Unit 6, is 4 m of well-sorted, fine to medium aeolian sand (Facies 4), which formed the current stabilized dune

landscape, and yielded bounding OSL ages of 425 ± 15 yr (BG4859) and 405 ± 15 yr (BG4858).

Core RR18-OK7 (34.22237°N, 99.16671°W, 357 m elevation, 7 m above RRL)

Core RR18-OK7 was taken from a proximal dune field at a prominent bend in the Red River (Fig. 2C). This core revealed 10.6 m of aeolian sand burying at least 1.5 m of fluvial sediment (Fig. 8D). The two basal fluvial units (1 and 2) are fining upward sequences of sands, granules, and gravels (Facies 1) capped by a paleosol. Quartz grains from the upper fluvial unit (2) yielded an OSL age of 7915 ± 360 yr (BG4903), marking a time of aggradation. Overlying the fluvial sand is a tripartite aeolian sequence with each unit (3–5) fining upward (Facies 3), with a buried cambic soil horizon demarking the upper contact of each unit. A series of five OSL ages from Units 3, 4, and 5 (Fig. 8D) indicate sand sheet deposition at ca. 6.5, 4.3 to 3.9, and 3.1 to 0.5 ka, respectively. The uppermost, 5-m-thick unit (6), which encompasses dunes expressed at the surface, is a well-sorted, medium to fine sand, mostly massive Facies 4-type sediment. Quartz grains from the base, midway, and near the top of Unit 6 returned OSL ages of 515 ± 20 yr (BG4899), 420 ± 40 yr (BG4898), and 395 ± 20 yr (BG4897), respectively, indicating near-continuous aeolian deposition at this site between ca. 520 and 350 yr ago.

DISCUSSION

Oldest ca. 85 to 65 ka fluvial and aeolian depositional record of the western Red River

The oldest recognized fluvial sediments are revealed in cores RRCOR16-1, RR18-OK1, and RR18-OK2, which returned OSL ages from 85 to 70 ka (Fig. 9). These fluvial sediments fine upward from Facies 1 to 2, with the top of the aggradational limit (falling stage) demarked by a buried soil or truncated by emplacement of younger fluvial gravels ca. 26 ka (Fig. 8C). Thus, there was net fluvial aggradation of at least 8 m between ca. 80 and 60 ka, as shown in cores RR18-OK1 and RR18-OK2 (Fig. 8C). However, the elevation of the paleo-surface revealed by Geoprobe cores RRCOR16-1 and RR18-OK1 at 7 to 8 m above RRL is a closer estimate of the terrace height (Fig. 10). The subsequent burial of the terrace by 5 to 7 m of aeolian sediments in the past 60 ka elevated the land surface in places, yielding an apparent height of 12 to 15 m for this terrace in places. We informally labeled this older remnant terrace at 5 to 8 m above the Red River and associated deposits that are ca. 85 to 65 ka old as “Vernon” for a nearby town (Figs. 1, 10, and 11).

Other fluvial deposits and river terraces have been identified in central and southern Texas that yield luminescence ages of ca. 80 to 65 ka consistent with the 7 to 8 m above RRL, buried Vernon surface. These fluvial deposits may be time equivalent with late Beaumont deposits along the Texas Coastal Plain emplaced during the transition from MIS 5 into cooling conditions in MIS 4 (Blum and Aslan, 2006). Similar OSL ages (ca. 72 to 64 ka) were reported for quartz grains from alluvial terrace (T2) sediments that host mammoth and other faunal remains at ~15 to 16 m above the Brazos River at the Waco Mammoth National Monument; and with abandonment of the terrace surface after ca. 52 ka (Nordt et al., 2015; Taormina et al., 2022). Another possible correlative deposit is an aggradational and truncated terrace (Q5) identified between 5 and 10 m above Owl Creek, a tributary

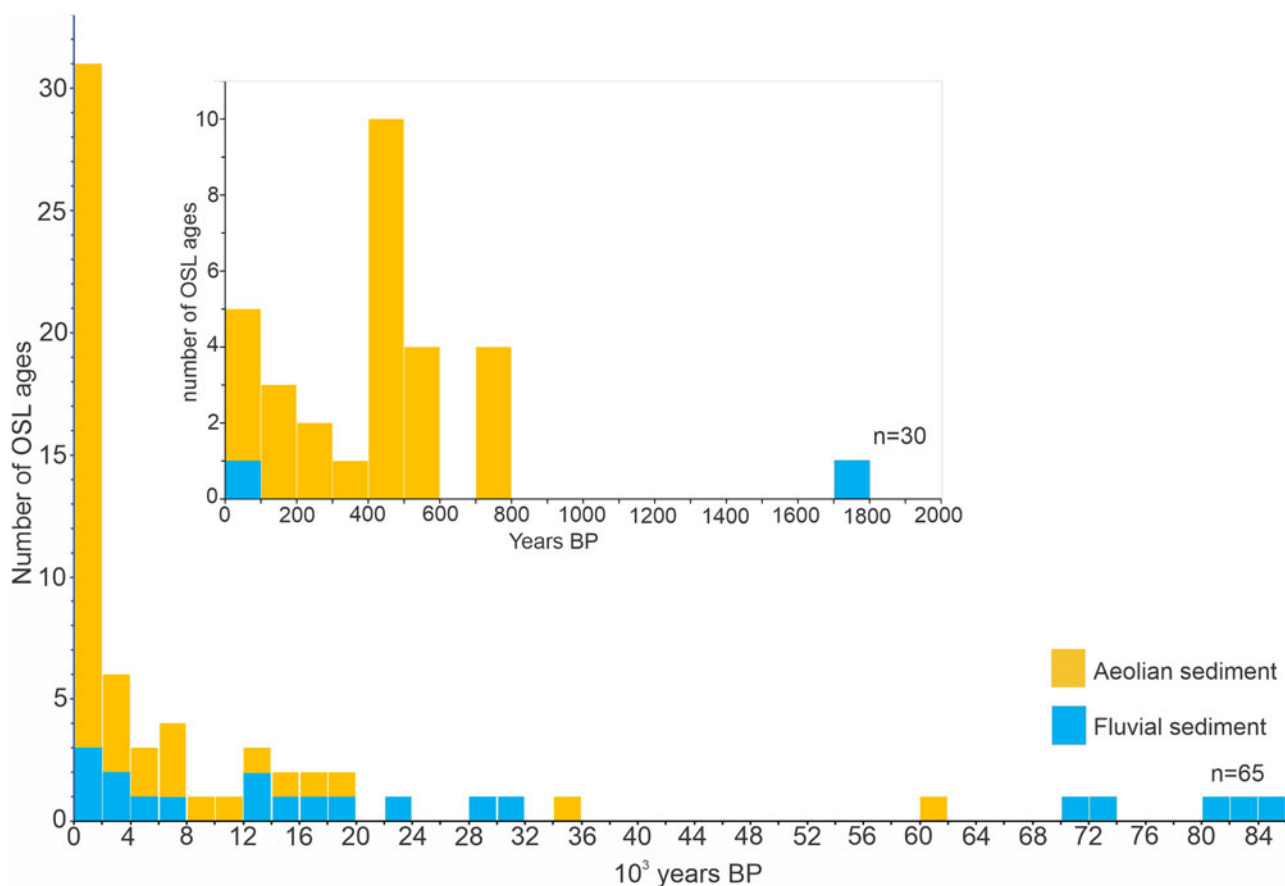


Figure 9. Frequency distribution of optically stimulated luminescence (OSL) ages for aeolian and fluvial sediments for western Red River study area.

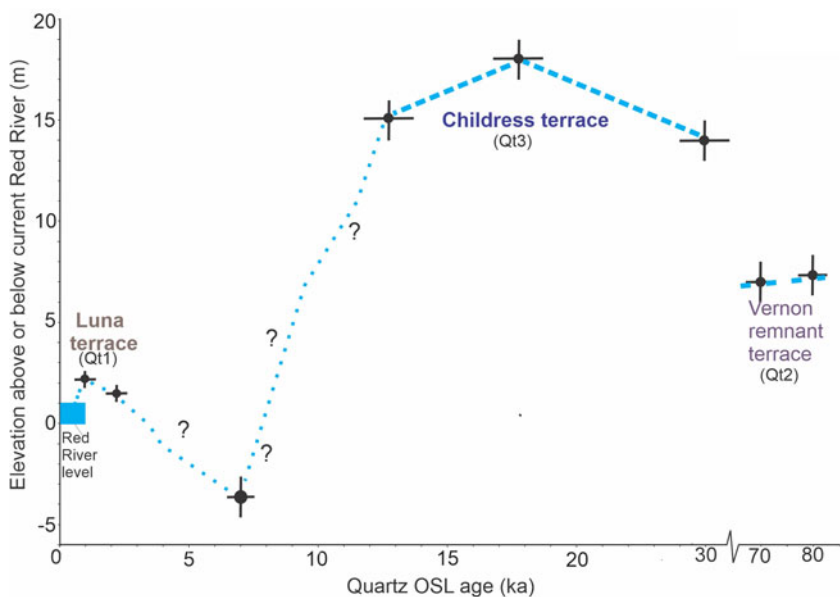


Figure 10. Inferred changes in Red River water level relative to current elevation in the past 80 ka. OSL, optically stimulated luminescence.

to the Brazos River, in central Texas with bracketing OSL ages of ca. 75 and 44 ka (Meier et al., 2013). These surfaces may also be penecontemporaneous with the late Prairie Complex of the lower to middle Mississippi River valley, a fluvial deposit that reflects mesic conditions, shoreline progradation, and subsequent degradation with the fall in global sea level during the MIS 5 to MIS

4 transition (Dorale et al., 2010), possibly associated with late fluvial incision (Shen et al., 2012). Also, this oldest recognized fluvial deposit for the Red River appears to be time equivalent (80 to 60 ka) with the transition between the Beaumont and the Deweyville Formations, reflecting a period of pronounced incision post-Beaumont time, and initial aggradation from Deweyville

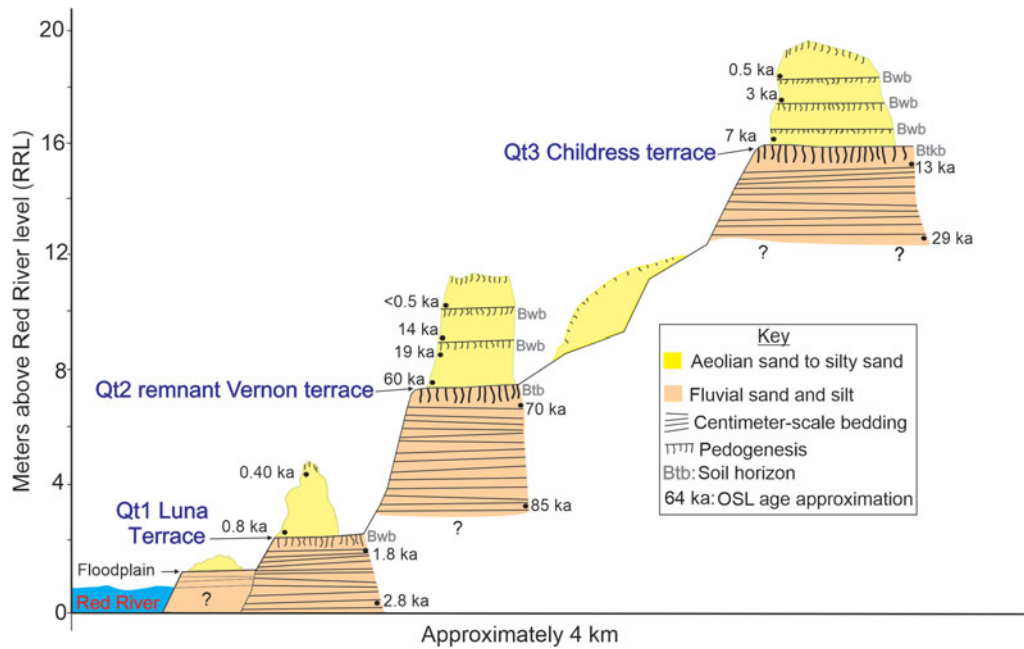


Figure 11. Diagrammatic cross section of western Red River terraces and fluvial and aeolian deposits with optically stimulated luminescence (OSL) age control.

surfaces along the Texas coast and associated inland fluvial systems (Blum and Aslan, 2006).

The oldest identified aeolian deposit is from core RR18-OK1 (Facies 3), as a <1-m-thick sandy silt (Facies 2) that yielded an OSL age of $60,210 \pm 3010$ yr BP (BG4960) (Figs. 8A and 9). This remnant, massive aeolian unit buries a truncated, well-developed buried soil (Btk horizon) formed in a fluvial deposit, with an OSL age of 72.2 ka (Fig. 8A), indicating that this buried soil has a maximum age span of ca. 12 ka, with terrace abandonment after 67 ka. In turn, this aeolian deposit was eroded with the deposition of the overlying aeolian sand ca. 37 ka. This period of aeolian deposition ca. 60 to 35 ka is consistent with a pronounced aeolian depositional phase in the Monahans dune field in west Texas burying a prominent paleosol and is associated with increased regional aridity (Forman *et al.*, 2022).

Little is known about the paleoenvironmental variability before the LGM in midcontinental North America, reflecting uncertainty about ice-sheet extent and dynamics (Dalton *et al.*, 2022). Sea level at ca. 80 ka during MIS 5a is constrained at or near levels similar to those today, though potentially short-lived for 5 to 10 ka (Dorale *et al.*, 2010), with nearly full deglaciation of the North American continent (Gowan *et al.*, 2021; Dalton *et al.*, 2022). Speleothem records from Crevice Cave, Missouri, show a series of short, positive oxygen isotope oscillations at ca. 74, 71, and 64 ka, reflecting 2°C to 3°C cooling events every 3 to 7 ka, with relative warming for intervening periods (Dorale *et al.*, 1998). Associated carbon isotopes and pollen indicate an increasing dominance of grassland with high C₄ biomass, an indication of drying (Dorale *et al.*, 1998; Baker *et al.*, 2009). Thus, the formation of the Vernon terrace between ca. 79 and 66 ka may be associated with repeated wet periods increasing runoff and subsequent dry conditions, and changing vegetation cover, all of which may have provided enhanced clastic inputs for net aggradation. Final downcutting and surface abandonment between 66 and 50 ka may be associated with regional aridity and cooling of North America and displacement of zonal circulation as the

Laurentide Ice Sheet advanced into the midcontinent (Schmidt and Hertzberg, 2011; Dalton *et al.*, 2022).

LGM fluvial and aeolian depositional complex

The highest fluvial sediments identified in cores RRCOR16-3 and RRCOR18-2 are 15 to 20 m above the current channel and yielded associated OSL ages from the LGM to the earliest Holocene, ca. 30 to 12 ka (Figs. 7 and 8B). Similar high-elevation fluvial terraces (>5 m above the current channel) with associated ages between 25 and 12 ka have been identified along the Brazos (Waters and Nordt, 1995; Taormina *et al.*, 2022) and the Pedernales Rivers (Blum and Valastro, 1994). This period of fluvial aggradation is associated with a regional positive water balance as indicated by the presence of paleo-Lake King in far western Texas (Wilkins and Currey, 1997), other pluvial lakes in New Mexico (Allen, 2005), and associated climate modeling (Lora and Ibarra, 2019). Wetter conditions, particularly in winter, are associated with maximum glaciation of North America, with several proxy records indicating the periodic strengthening of zonal precipitation in the southwestern United States (Bartlein *et al.*, 2011; Bhattacharya *et al.*, 2018; Izumi *et al.*, 2022), which would enhance sediment delivery into catchments during a season with low vegetation cover, resulting in pronounced aggradation (e.g., Waters *et al.*, 2021).

Three cores—RR16-1, RR16-3, and RR18-OK1—show modest aeolian deposition during the LGM, ca. 25 to 13 ka (Figs. 7 and 8). These aeolian deposits are massive, moderately well-sorted, cover sands to loams, ≤ 1 m thick. In core RR18-OK1, the thin Unit 6 that yielded the basal OSL age of 14.3 ka is capped by a cambic horizon demarcating the end of the LGM (Fig. 8A).

Of note, the highest preserved Childress terrace at 15 to 20 m, with OSL ages of ca. 30 to 14 ka old, is not the oldest identified fluvial deposit. The oldest preserved fluvial sediment is associated with the Vernon terrace, 85 to 70 ka old, and often occurs beneath 3 to 4 m thickness of aeolian sediments, with a terrace top at 7 to

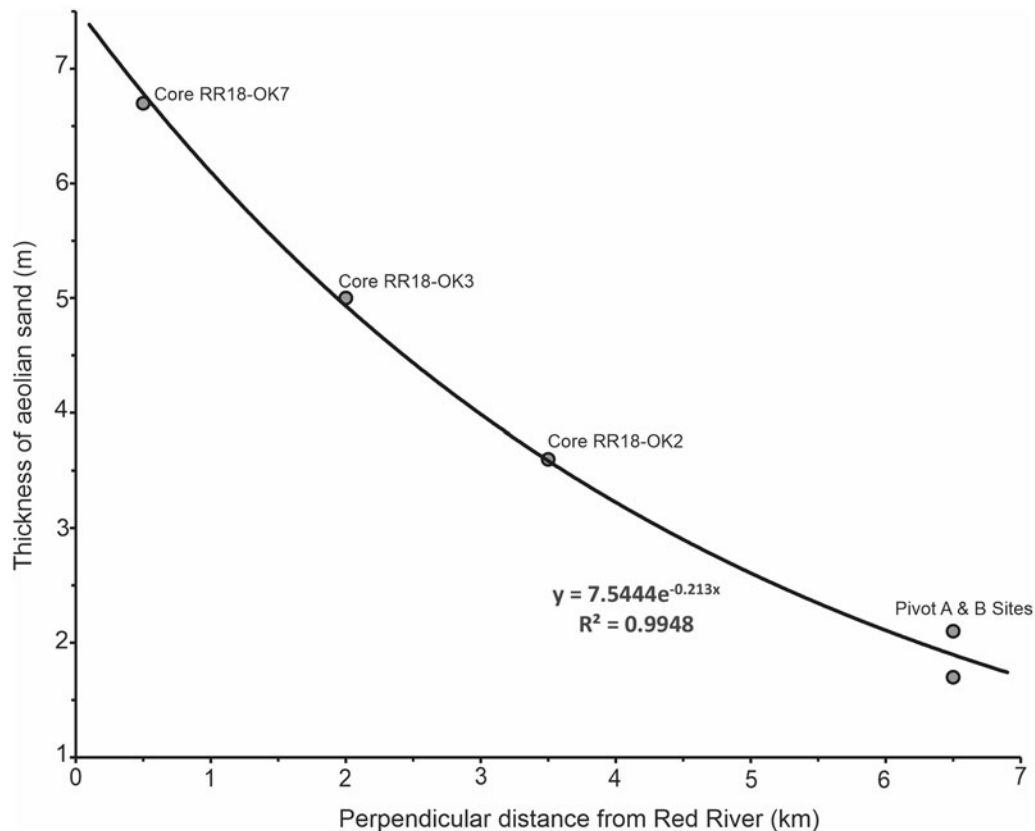


Figure 12. Thickness of aeolian sediments dated between 550 and 300 yr ago in reference to perpendicular distance to the Red River. The thickness of this sedimentary unit thins exponentially from the River Red source onto adjacent terraces.

8 m, a lower elevation of the Childress terrace. The Vernon terrace is unpaired and reflects greater lateral migration than downcutting in the past 70 ka (Bierman and Montgomery, 2014, pp. 235–237) and preservation beneath >3-m-thick aeolian and fluvial deposits. Similar unpaired terraces and terrace remnants have been found for terraces and strath surfaces along the Colorado Front Range, reflecting complex channel dynamics with multiple reoccupations of river levels, variable channel migration, and erosion during the late Pleistocene (e.g., Dühnforth et al., 2012; Foster et al., 2017).

Holocene fluvial degradation and aggradation and aeolian deposition

There is an absence of recognized fluvial deposits from the Early to Middle Holocene, ca. 17.0 to 7.0 ka (Fig. 9). The oldest identified Holocene fluvial deposit yielded an OSL age of 7015 ± 360 yr (BG4903) from core RR18-OK7 (Fig. 8), proximal to the Red River, at about 4 m below the current river elevation. Though limited, these observations indicate that much of the early Holocene may have been a period of net fluvial degradation of ~20 m, from a height of 14 to 16 m above the current Red River at ca. 13 ka to at least 4 m below the channel by 7 to 6 ka (Fig. 10). However, after ca. 7 ka at the RR18-OK7 core site, aggradation or channel abandonment occurred, as indicated by basal fluvial sediments (Facies 2) capped by buried soils. In turn, overlying fluvial Unit 2 are >4 m thickness of sand sheet sediments (Facies 3) deposited between 6.5 and 0.5 ka (Fig. 8D). The deposition of this aeolian sand sheet occurred episodically at ca. 6.5 to ~4.6 ka, 4.3 to ~3.8 ka, and 3.2 to 0.5 ka, with OSL ages indicating that the

bounding, well-drained, cambic buried soils reflect hiatuses of <2000 yr (Fig. 8D).

Fluvial aggradation continued into the Late Holocene from 4.0 to 1.5 ka, as shown in core RR18-OK3. This succession from channel gravels to overbank silts and sands (Facies 1 to 2) with a capping buried soil (Fig. 8C) indicates an aggradational limit and subsequent downcutting and/or abandonment of this fluvial surface (Fig. 11). Unconformably overlying these fluvial sediments is a <10-m-thick sequence of aeolian sand deposited between 600 and 300 yr ago. This Qt1 surface, informally named the “Luna” terrace, occurs 1 to 3 m above RRL and formed between ca. 1500 and 700 yr ago. The lowest and youngest recognized fluvial deposits at the Mike Site (Fig. 2A), are inset into the Luna terrace at 1.5 m RRL and yield OSL ages from 150 to 30 yr old (Fig. 6B), which shows nineteenth- and twentieth-century fluvial accretion and later incision. In turn, the Hollis Site, also at the current cutbank of the Red River (Fig. 2A), shows the association of aeolian of sand sheet deposited ca. 195 to 10 yr ago (Fig. 6C), sourced from the immediately adjacent floodplain surface, as inferred for earlier aeolian deposits at ca. 500 to 400 yr ago.

Little Ice Age, 500 to 400 years ago, source-border dune fields

A compelling result is the latest and most pronounced phase(s) of aeolian deposition occurred between 550 and 400 yr ago at most study sites (Figs. 6–8). This phase is recognized in cores and sections as a 1.7- to 2.0-m-thick deposit on the highest surfaces distal (6.5 km) from the Red River and thickens exponentially to 7 to

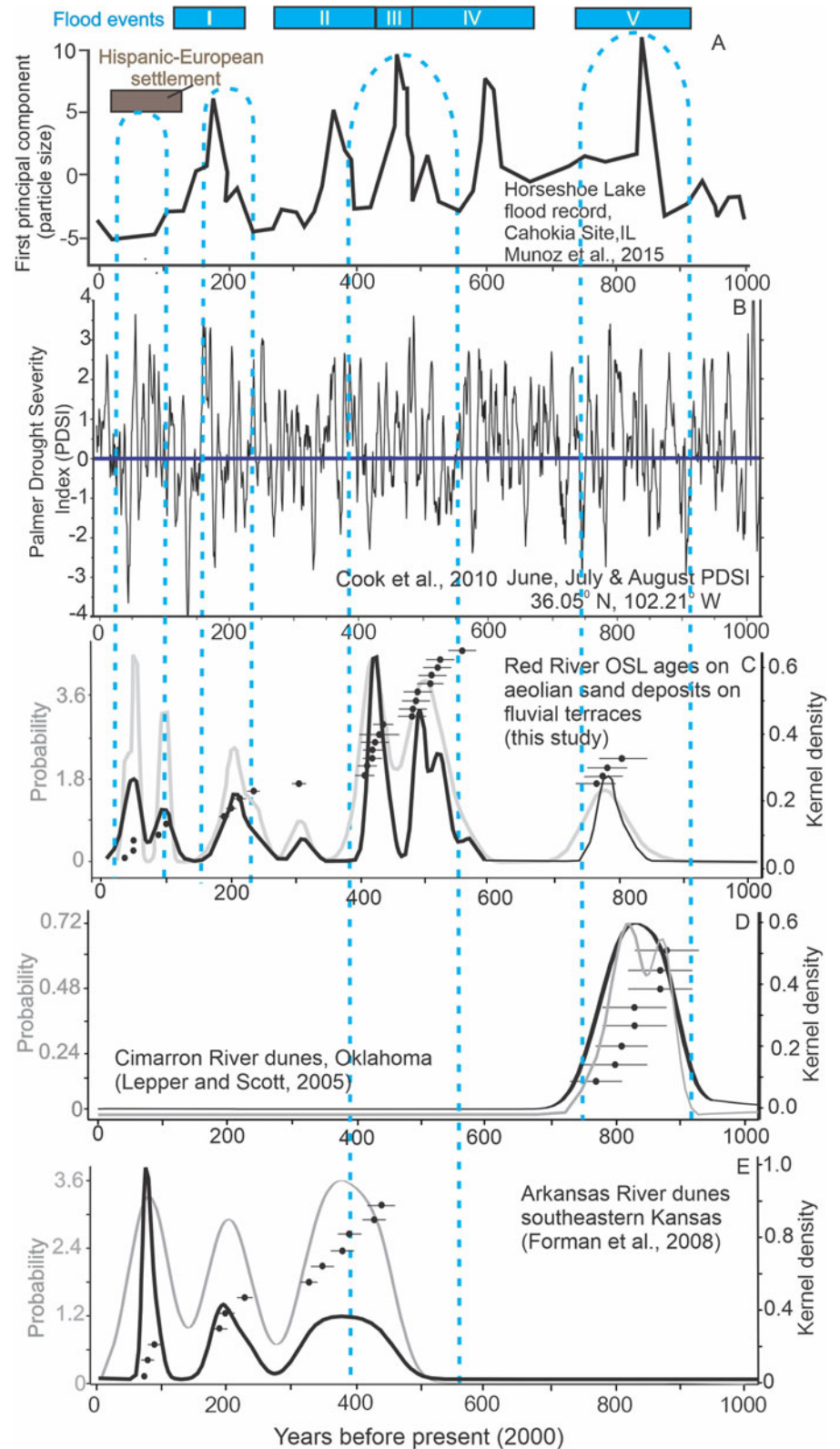


Figure 13. Comparison of proxy environmental records for the past 1000 yr. (A) Mississippi River paleoflood record from Horseshoe Lake, near Cahokia Site, IL (Munoz et al., 2015). (B) June, July, and August Palmer Drought Severity Index for headwaters of the Red River in the Sangre de Cristo Mountains, NM (Cook et al., 2010). (C) Distribution of optically stimulated luminescence (OSL) ages on aeolian sand deposits on fluvial terraces, western Red River (this study). (D) Distribution of OSL ages for aeolian sand deposits associated with Cimarron River, OK (Lepper and Scott, 2005). (E) Distribution of OSL ages for aeolian sand deposits associated with Arkansas River dunes, southeastern Kansas (Forman et al., 2008).

5 m at sites <2 km perpendicular distance from the river (Fig. 12), indicating a riverine source for this aeolian sediment. The exponential decrease in aeolian sand thickness that yielded OSL ages between 550 and 400 yr is similar to the decrease in Peoria loess thickness from bluff edges in the Mississippi and Missouri

valleys proximal to this aeolian sediment source (Rodbell et al., 1997; Muhs et al., 2008).

Aeolian deposition in the past 500 yr shows two potential sub-phases at its thickest stratigraphic occurrence in cores RR18-OK2 and RR18-OK3, and identified traceable units in the Pivot A and

B sections with initial aeolian deposition occurred at ca. 550 to 450 yr BP. A later subphase of aeolian deposition spanned from 420 to 380 yr ago and was separated from the earlier phase by a distinct cambic buried soil. The apparent sedimentation rate of 11 to 4 cm/yr associated with these phases of aeolian deposition are similar in magnitude to other source-border aeolian systems associated with coastal settings (e.g., Maun, 2009, p. 96; Han et al., 2021), further underscoring a proximal riverine source for aeolian sediments.

The latest phase of aeolian deposition occurs between AD 1590 and AD 1620 and appears to coincide with a comparatively wet period in the central United States associated with Little Ice Age cooling in the Northern Hemisphere (Cook et al., 2016). This period of aeolian deposition may also partially overlap with or closely follow, considering errors in OSL ages, a sixteenth-century megadrought between AD 1570 and AD 1590 (Stahle et al., 2007; Cook et al., 2018). Landscape denudation associated with a regional drought can yield pronounced sediment delivery into adjacent fluvial systems, particularly if followed by excess runoff with pluvial conditions, leading to aggradation (Hall, 1990) and enhanced fluvial sediment supply for aeolian transport in channel proximal dunes. A pronounced dune accretion phase 300 to 500 yr ago has also been identified along the Arkansas River valley in western and eastern Kansas (Arbogast, 1996; Forman et al., 2008; Halfen, 2012). The closest tree ring-based Palmer Drought Severity Index (PDSI) record is near the headwaters of the Red River in the Sangre de Cristo Mountains and shows a pronounced wet interval for the late sixteenth and seventeenth centuries (Fig. 13). This record shows wet years with PDSI values up to +4 often separated by years with PDSI values ranging from 0.5 to -2.0. These inferred wet years may be coincident with flood years inferred for the middle Mississippi River valley from core records for an oxbow lake (Munoz et al., 2015, 2018; Fig. 13). Flood and/or high discharge events would provide added sediment supply across the Red River valley that would become available with waning flood stage and subsequent drying (e.g., Sankey et al., 2018). Thus, aeolian deposition in the late sixteenth and early seventeenth centuries is associated with wetter conditions providing new sources of sediment for river-proximal aeolian deposition on adjacent terraces. Subsequent reactivation of aeolian systems 200 and 90 yr ago may be associated with the Civil War and 1930s Dust Bowl Droughts with heightened anthropogenic activity (Woodhouse et al., 2002; Bolles et al., 2019).

CONCLUSION

Geomorphic mapping identified three distinct terraces levels up to 15 to 20 m above the Red River, often covered by 2 to 8 m of aeolian sand forming presently stabilized source-border dune fields (Fig. 11). Pedostratigraphic, granulometric, carbonate content analysis in tandem with OSL-SAR dating of quartz grains from four stratigraphic sections and six Geoprobe cores from terraces covered by aeolian deposits provide new insights into the relation between fluvial dynamics and aeolian depositional phases (Figs. 11 and 13). The oldest fluvial landform, ca. 80 ka old, covered by 3 to 6 m of aeolian sand, is informally named the Vernon terrace, which occurs at 5 to 8 m above the current Red River. The Vernon terrace occurs as a remnant and may be associated with hydrologic variability during the transition from interglacial to glacial conditions ca. 85 to 65 ka, with enhanced clastic input for net aggradation. This surface was abandoned and incised

sometime between 70 and 60 ka possibly in association with inferred regional aridity and cooling with the advance of the Laurentide Ice Sheet into the midcontinent of North America (Dorale et al., 1998; Dalton et al., 2022).

The highest fluvial sediments identified are 15 to 20 m above the current Red River and yielded OSL ages of between 30 and 13 ka and capped in places by 4 to 5 m thickness of Holocene aeolian sediments (Fig. 11). This surface has been informally named the Childress terrace and is associated with an extended ca. 15 ka period with net fluvial aggradation. This period appears coincident with regional positive water balance with highstands of pluvial lakes in west Texas and adjacent New Mexico (Wilkins and Currey, 1997). Aeolian deposition appears to be sparse during the LGM on Red River terraces, with the uncommon occurrence of 1 to 2 m of pedogenically modified cover loam and sand.

There is a noticeable absence of fluvial deposits with OSL ages between 12.0 and 7.0 ka (Fig. 9). The oldest identified Holocene fluvial deposit is 7 ka old and occurs ~4 m below the current river channel. Thus, the Early to Middle Holocene was a time of net fluvial degradation of 15 to 20 m from the Childress terrace (Figs. 10 and 11), associated potentially with regional aridity with lowering of groundwater level. However, sometime between 7 and 1 ka, there was net aggradation to about 2 m RRL, forming the Luna terrace surface, with abandonment sometime between 1.5 and 0.7 ka (Fig. 11). Aeolian sediments, 4 to 10.5 m thick and spanning from 6.5 to 0.2 ka, were deposited on terrace surfaces (Fig. 11), with thickness dependent on the proximity to the riverine source (Fig. 12).

A compelling result is that dune accretion across terraces occurred between 500 and 300 yr ago with an apparent sedimentation rate of 11 to 3 cm/yr, similar in magnitude to coastal aeolian systems (e.g., Maun, 2009, p. 96; Han et al., 2021), thus underscoring a proximal riverine source for the Red River dune fields. A pronounced dune accretion phase 300 to 500 yr ago has also been identified along the Arkansas River valley in western and eastern Kansas (Arbogast, 1996; Forman et al., 2008; Halfen, 2012; Halfen et al., 2012). This sixteenth- and seventeenth-century phase of dune building occurred during a comparatively cool and wet period in the central United States, the Little Ice Age, and is coincident with major flood intervals in the middle Mississippi River (Munoz et al., 2015, 2018; Fig. 13). Sediment availability and sources for aeolian transport were heightened post high river discharge and flood events exposing sand and silt-rich fluvial surfaces as sources to accrete dune systems on river proximal terraces. Fluvial source-border dune fields adjacent to the Red River and other rivers on the SGP may reflect hydrologic variability with flooding rather than the common and counterinterpretation of drought or megadrought conditions (Forman et al., 1995, 2001, 2008; Hanson et al., 2010; Halfen and Johnson, 2013; Halfen et al., 2016).

Supplementary Material. The supplementary material for this article can be found at <https://doi.org/10.1017/qua.2023.15>.

Acknowledgments. This research was supported initially through grants from the National Science Foundation (award GSS-1660230) and the National Geographic Society (no. 9990-16). Access to study sites was generously provided by local landowners on both sides of the state boundary. Discussions with M. Waters, who freely shared his knowledge, were enlightening. Comments from two anonymous reviewers and the editors were appreciated and improved the presentation. Each study reveals partially, and all shortcomings are solely the responsibility of the authors.

REFERENCES

- Alizai, A., Carter, A., Clift, P.D., Van Laningham, S., Williams, J.C., Kumar, R., 2011. Sediment provenance, reworking and transport processes in the Indus River by U-Pb dating of detrital zircon grains. *Global Planetary Change* 76, 33–55.
- Allen, B.D., 2005. Ice Age lakes in New Mexico. In: Lucas, S.G., Morgan, G.S., Zeigler, K.E. (Eds.), *New Mexico's Ice Ages. New Mexico Museum of Natural History and Science Bulletin*, no. 28, 107–114.
- Arbogast, A.F., 1996. Stratigraphic evidence for late-Holocene aeolian sand mobilization and soil formation in south-central Kansas, USA. *Journal of Arid Environments* 34, 403–414.
- Aslan, A., Autin, W.J., 1998. Holocene flood-plain soil formation in the southern lower Mississippi Valley: Implications for interpreting alluvial paleosols. *Geological Society of America Bulletin* 110, 433–449.
- Autin, W.J., 1996. Pleistocene stratigraphy in the southern lower Mississippi Valley. *Engineering Geology* 45, 87–112.
- Autzen, M., Andersen, C.E., Bailey, M. Murray, A.S., 2022. Calibration quartz: an update on dose calculations for luminescence dating. *Radiation Measurements* 157, 106828.
- Baker, R.G., Bettis, E.A., Mandel, R.D., Dorale, J.A., Fredlund, G.G., 2009. Mid-Wisconsinan environments on the eastern Great Plains. *Quaternary Science Reviews* 28, 873–889.
- Barchyn, T.E., Hugenholtz, C.H., 2012. A process-based hypothesis for the barchan-parabolic transformation and implications for dune activity modelling. *Earth Surface Processes* 37, 1456–1462.
- Bartlein, P.J., Harrison, S.P., Brewer, S., Connor, S., Davis, B.A.S., Gajewski, K., Guiot, J., et al., 2011. Pollen-based continental climate reconstructions at 6 and 21 ka: a global synthesis. *Climate Dynamics* 37, 775–802.
- Bertrand, D., McPherson, R.A., 2018. Future hydrologic extremes of the Red River basin. *Journal of Applied Meteorology and Climatology* 57, 1321–1336.
- Bhattacharya, T., Tierney, J.E., Addison, J.A., Murray, J.W., 2018. Ice-sheet modulation of deglacial North American monsoon intensification. *Nature Geoscience* 11, 848–852.
- Bierman, P.R., Montgomery, D.R., 2014. *Key Concepts in Geomorphology*. Freeman, New York.
- Birkeland, P.W., 1999. *Soils and Geomorphology*. 3rd ed. Oxford University Press, New York.
- Blum, M.D., Aslan, A., 2006. Signatures of climate vs. sea-level change within incised valley-fill successions: Quaternary examples from the Texas Gulf Coast. *Sedimentary Geology* 190, 177–211.
- Blum, M.D., Toomey, R.S., III, Valastro, S., Jr., 1994. Fluvial response to Late Quaternary climatic and environmental change, Edwards Plateau, Texas. *Palaeogeography, Palaeoclimatology, Palaeoecology* 108, 1–21.
- Blum, M.D., Valastro, S., 1994. Late Quaternary Sedimentation, Lower Colorado River, Gulf Coastal-Plain of Texas. *Geological Society of America Bulletin* 106, 1002–1016.
- Bolles, K., Forman, S.L., Sweeney, M., 2017. Eolian processes and heterogeneous dust emissivity during the 1930s Dust Bowl Drought and implications for projected 21st-century megadroughts. *The Holocene* 27, 578–1588.
- Bolles, K., Sweeney, M., Forman, S.L., 2019. Meteorological conditions and particle source dynamics for dust storms during the 1930s “Dust Bowl” drought, Southern High Plains, USA. *Anthropocene* 27, 100216.
- Bullard, J.E., McTainsh, G.H., 2003. Aeolian-fluvial interactions in dryland environments: examples, concepts and Australia case study. *Progress in Physical Geography: Earth and Environment* 27, 471–501.
- Cook, B.I., Cook, E.R., Smerdon, J.E., Seager, R., Williams, A.P., Coats, S., Stahle, D.W., Diaz, J.V., 2016. North American megadroughts in the Common Era: reconstructions and simulations. *Wiley Interdisciplinary Reviews: Climate Change* 7, 411–432.
- Cook, B.I., Williams, A.P., Smerdon, J.E., Palmer, J.G., Cook, E.R., Stahle, D.W. Coats, S., 2018. Cold tropical Pacific Sea surface temperatures during the late sixteenth-century North American megadrought. *Journal of Geophysical Research: Atmospheres* 123, 11307–11320.
- Cook, E.R., Seager, R., Heim, R.R., Vose, R.S., Herweijer, C., Woodhouse, C., 2010. Megadroughts in North America: analyzing IPCC projections of hydroclimatic change in a long-term palaeoclimate context. *Journal of Quaternary Science* 25, 48–61.
- Cordova, C.E., Porter, J.C., Lepper, K.E., Kalchgruber, R., Scott, G.F., 2005. Preliminary assessment of sand dune stability along a bioclimatic gradient, north-central and north-central and northwestern Oklahoma. *Great Plains Research* 15, 227–249.
- Dalton, A.S., Stokes, C.R., Batchelor, C.L., 2022. Evolution of the Laurentide and Innuitian ice sheets prior to the Last Glacial Maximum (115 ka to 25 ka). *Earth-Science Reviews* 224, 103875.
- Dorale, J.A., Edwards, R.L., Ito, E., Gonzalez, L.A., 1998. Climate and vegetation history of the midcontinent from 75 to 25 ka: a speleothem record from Crevice Cave, Missouri, USA. *Science* 282, 1871–1874.
- Dorale, J.A., Onac, B.P., Fornos, J.J., Gines, J., Gines, A., Tuccimei, P., Peate, D.W., 2010. Sea-level highstand 81,000 years ago in Mallorca. *Science* 327, 860–863.
- Draut, A.E., 2012. Effects of river regulation on aeolian landscapes, Colorado River, southwestern USA. *Journal of Geophysical Research: Earth Surface* 117. <https://doi.org/10.1029/2011JF002329>.
- Dühnforth, M., Anderson, R.S., Ward, D.J., Blum, A., 2012. Unsteady late Pleistocene incision of streams bounding the Colorado Front Range from measurements of meteoric and in situ ¹⁰Be. *Journal of Geophysical Research: Earth Surface* 117(F1). <https://doi.org/10.1029/2011JF002232>.
- Edwards, W.D., 2016. River Channel Monitoring of the Red River of the Texas and Oklahoma State Boundary, USA, Using Remote Sensing Techniques and the Legal Implications on Riparian Boundaries. PhD dissertation, University of Texas at Dallas, Dallas, TX.
- Fisk, H.N., 1938. *Geology of Grant and La Salle Parishes. Louisiana Geological Survey, Geological Bulletin*, no. 10.
- Folk, R.L., 1980. *Petrology of Sedimentary Rocks*. Hemphills Publishing, Austin, TX.
- Forman, S.L., Marin, L., Gomez, J., Pierson, J., 2008. Late Quaternary eolian sand depositional record for southwestern Kansas: landscape sensitivity to droughts. *Palaeogeography, Palaeoclimatology, Palaeoecology* 265, 107–120.
- Forman, S.L., Oglesby, R., Markgraf, V., Stafford, T., 1995. Paleoclimatic significance of Late Quaternary eolian deposition on the Piedmont and High Plains, Central United States: *Global and Planetary Change* 11, 35–55.
- Forman, S.L., Oglesby, R., Webb, R.S., 2001. Temporal and spatial patterns of Holocene dune activity on the Great Plains of North America: megadroughts and climate links: *Global and Planetary Change* 29, 1–29.
- Forman, S.L., Tew-Todd, V., Mayhack, C. Wiest, L. A., Money, G., 2022. Late Quaternary aeolian environments, luminescence chronology and climate change for the Monahans dune field, Winkler County, West Texas, USA. *Aeolian Research* 58, 100828.
- Foster, M., Anderson, R., Gray, H., Mahan, S., 2017. Dating of river terraces along Lefthand Creek, western High Plains, Colorado, reveals punctuated incision. *Geomorphology* 295, 176–190.
- Fryberger, S.G., 1979. Dune forms and wind regime. In: Mckee, E.D. (Ed.), *A Study of Global Sand Seas*. U.S. Geological Survey Professional Paper 1052. U.S. Government Printing Office, Washington, DC, pp. 137–169.
- Frye, J.C., Leonard, A.B., 1963. *Pleistocene Geology of Red River Basin in Texas*. Report of Investigations No. 49. Bureau of Economic Geology, University of Texas, Austin, TX.
- Galbraith, R.F., Roberts, R.G., 2012. Statistical aspects of equivalent dose and error calculation and display in OSL dating: an overview and some recommendations. *Quaternary Geochronology* 11, 1–27.
- Galbraith, R.F., Roberts, R.G., Laslett, G.M., Yoshida, H., Olley, J.M., 1999. Optical dating of single and multiple grains of quartz from Jinmium rock shelter, northern Australia, part 1, Experimental design and statistical models. *Archaeometry* 41, 339–364.
- Gowan, E.J., Zhang, X., Khosravi, S., Rovere, A., Stocchi, P., Hughes, A.L.C., Gyllencreutz, R., Mangerud, J., Svendsen, J.-I., Lohmann, G., 2021. A new global ice sheet reconstruction for the past 80 000 years. *Nature Communications* 12, 1199.
- Halfen, A.F., 2012. Medieval Climatic Anomaly and Little Ice Age dune activity in the Arkansas River Valley, Central Great Plains, USA. *Quaternary International* 279–280, 185.
- Halfen, A.F., Johnson, W.C., 2013. A review of Great Plains dune field chronologies. *Aeolian Research* 10, 135–160.

- Halfen, A.F., Johnson, W.C., Hanson, P.R., Woodburn, T.L., Young, A.R., Ludvigson, G.A., 2012. Activation history of the Hutchinson dunes in east-central Kansas, USA during the past 2200 years. *Aeolian Research* 5, 9–20.
- Halfen, A.F., Lancaster, N., Wolfe, S., 2016. Interpretations and common challenges of aeolian records from North American dune fields. *Quaternary International* 410, 75–95.
- Hall, S.A., Goble, R.J., 2012. Berino paleosol, Late Pleistocene argillic soil development on the Mescalero sand sheet in New Mexico. *Journal of Geology* 120, 333–345.
- Han, M., Kim, J.C., Yang, D.Y., Lim, J., Yi, S., 2021. The main periods and environmental controls of coastal dune development along the west coast of the Korean Peninsula during the mid to late Holocene. *Palaeogeography, Palaeoclimatology, Palaeoecology* 569, 110345.
- Hanson, P.R., Arbogast, A.F., Johnson, W.C., Joeckel, R.M., Young, A.R., 2010. Megadroughts and late Holocene dune activation at the eastern margin of the Great Plains, north-central Kansas, USA. *Aeolian Research* 1, 101–110.
- Holliday, V.T., 1995. Stratigraphy and Paleoenvironments of Late Quaternary Valley Fills on the Southern High Plains. *Geological Society of America Memoir* 186.
- Holliday, V.T., 2001. Stratigraphy and geochronology of upper Quaternary eolian sand on the Southern High Plains of Texas and New Mexico, United States. *Geological Society of America Bulletin* 113, 88–108.
- Houser, C., Bishop, M.P., Barrineau, P., 2015. Characterizing instability of aeolian environments using analytical reasoning. *Earth Surface Processes and Landforms* 40, 696–705.
- Hugenholtz, C.H., Koenig, D.K., 2014. Sand dune stabilization reduces infiltration and soil moisture: a case study from the northern Great Plains. *Ecology* 7, 1135–1146.
- Huggins, X., Gleeson, T., Kumm, M., Zipper, S.C., Wada, Y., Troy, T.J., Famiglietti, J.S., 2022. Hotspots for social and ecological impacts from freshwater stress and storage loss. *Nature Communications* 13, 439.
- Izumi, K., Valdes, P., Ivanovic, R., Gregoire, L., 2022. Impacts of the PMIP4 ice sheets on Northern Hemisphere climate during the last glacial period. *Climate Dynamics*. <https://doi.org/10.1007/s00382-022-06456-1>.
- Kocurek, G., Lancaster, N., 1999. Aeolian system sediment state: theory and Mojave Desert Kelso dune field example. *Sedimentology* 46, 505–515.
- Lancaster, N., Tchakerian, V.P., 2003. Late Quaternary eolian dynamics. In: Enzell, Y., Wells, S.G., Lancaster, N. (Eds.), *Paleoenvironments and Paleohydrology of the Mohave and Southern Great Basin Deserts*. *Geological Society of America Special Paper* 368, 231–249.
- Lepper, K., Scott, G.F., 2005. Late Holocene aeolian activity in the Cimarron River valley of west-central Oklahoma. *Geomorphology* 70, 42–52.
- Liang, P., Forman, S.L., 2019. LDAC: an Excel-based program for luminescence equivalent dose and burial age calculations. *Ancient TL* 37, 21–40.
- Liu, B.L., Coulthard, T.J., 2015. Mapping the interactions between rivers and sand dunes: implications for fluvial and aeolian geomorphology. *Geomorphology* 231, 246–257.
- Lora, J.M., Ibarra, D.E., 2019. The North American hydrologic cycle through the last deglaciation. *Quaternary Science Reviews* 226, 105991.
- Luna, M.C.de.M., Parteli, E.J.R., Durán, O., Herrmann, H.J., 2011. Model for the genesis of coastal dune fields with vegetation. *Geomorphology* 129, 215–224.
- Lundelius, E.L., Bryant, V.M., Mandel, R., Thies, K.J., Thoms, A., 2013. The first occurrence of a Toxodont (Mammalia Notoungulata) in the United States. *Journal of Vertebrate Paleontology* 33, 229–232.
- Lundelius, E.L., Thies, K.J., Graham, R.W., Bell, C.J., Smith, G.J., DeSantis, L.R.G., 2019. Proboscidea from the Big Cypress Creek fauna, Deweyville Formation, Harris County, Texas. *Quaternary International* 530, 59–68.
- Mangan, J.M., Overpeck, J.T., Webb, R.S., Wessman, C., Goetz, A.F.H., 2004. Response of Nebraska Sand Hills natural vegetation to drought, fire, grazing, and plant functional type shifts as simulated by the century model. *Climatic Change* 63, 49–90.
- Marin, L.C., Forman, S.L., Todd, V.T., Mayhack, C., Gonzalez, A., Peng, L., 2021. Isolation of quartz grains for optically stimulated luminescence (OSL) dating of Quaternary sediments for paleoenvironmental research. *Journal of Visual Experiments* 174, e62706.
- Maun, M.A., 2009. *The Biology of Coastal Sand Dunes*. Oxford University Press, New York.
- Meier, H.A., Nordt, L.C., Forman, S.L., Driese, S.G., 2013. Late Quaternary alluvial history of the middle Owl Creek drainage basin in central Texas: a record of geomorphic response to environmental change. *Quaternary International* 306, 24–41.
- Miall, A.D., 1996. *The Geology of Fluvial Deposits: Sedimentary Facies, Basin Analysis*. *Petroleum Geology*. Springer-Verlag, New York.
- Muhs, D.R., 2017. Evaluation of simple geochemical indicators of aeolian sand provenance: Late Quaternary dune fields of North America revisited. *Quaternary Science Reviews* 171, 260–296.
- Muhs, D.R., Bettis, E.A., Aleinikoff, J.N., McGeehin, J.P., Beann, J., Skipp, G., Marshall, B.D., Roberts, H.M., Johnson, W.C., Benton, R., 2008. Origin and paleoclimatic significance of late Quaternary loess in Nebraska: Evidence from stratigraphy, chronology, sedimentology, and geochemistry. *Geological Society of America Bulletin* 120, 1378–1407.
- Muhs, D.R., Reynolds, R.L., Been, J., Skipp, G., 2003. Eolian sand transport pathways in the southwestern United States: Importance of the Colorado River and local sources. *Quaternary International* 104, 3–18.
- Munoz, S.E., Giosan, L., Therrell, M.D., Remo, J.W., Shen, Z., Sullivan, R.M., Wiman, C., O'Donnell, M., and Donnelly, J.P., 2018. Climatic control of Mississippi River flood hazard amplified by river engineering. *Nature* 556, 95–98.
- Munoz, S.E., Gruley, K.E., Massie, A., Fike, D.A., Schroeder, S., Williams, J.W., 2015. Cahokia's emergence and decline coincided with shifts of flood frequency on the Mississippi River. *Proceedings of the National Academy of Science USA* 112, 6319–6324.
- Murray, A.S., Wintle, A.G., 2003. The single aliquot regenerative dose protocol: potential for improvements in reliability. *Radiation Measurements* 37, 377–381.
- Nordt, L., Bongino, J., Forman, S., Esker, D., Benedict, A., 2015. Late Quaternary environments of the Waco Mammoth site, Texas USA. *Quaternary Research* 84, 423–438.
- Otvos, E.G., 2013. Rapid and widespread response of the Lower Mississippi River to eustatic forcing during the last glacial-interglacial cycle: discussion. *Geological Society of America Bulletin* 125, 1369–1374.
- Prescott, J.R., Hutton, J.T., 1994. Cosmic ray contributions to dose rates for luminescence and ESR Dating: Large depths and long-term time variations. *Radiation Measurements* 23, 497–500.
- Qiao, L., Zou, C.B., Gaitán, C.F., Hong, Y., McPherson, R.A., 2017. Analysis of Precipitation Projections over the Climate Gradient of the Arkansas Red River Basin. *Journal of Applied Meteorology and Climatology* 56, 1325–1336.
- Rittenour, T.M., Blum, M.D., Goble, R.J., 2007. Fluvial evolution of the lower Mississippi River valley during the last 100 ky glacial cycle: response to glaciation and sea-level change. *Geological Society of America Bulletin* 119, 586–608.
- Rodbell, D.T., Forman, S.L., Pierson, J., Lynn, W.C., 1997. Stratigraphy and chronology of Mississippi Valley loess in western Tennessee. *Geological Society of America Bulletin* 109, 1134–1148.
- Routson, C.C., Overpeck, J.T., Woodhouse, C.A. Kenney, W.F., 2016. Three millennia of southwestern North American dustiness and future implications. *PLoS ONE* 11, 0149573.
- Sankey, J.B., Caster, J., Kasprak, A., East, A.E., 2018. The response of source-bordering aeolian dunefields to sediment-supply changes 2: controlled floods of the Colorado River in Grand Canyon, Arizona, USA. *Aeolian Research* 32, 154–169.
- Schmeisser, R.L., Loope, D.B., Mason, J.A., 2010. Modern and late Holocene wind regimes over the Great Plains (central U.S.A.). *Quaternary Science Reviews* 29, 554–566.
- Schmidt, M., Hertzberg, J., 2011. Abrupt climate change during the last Ice Age. *Nature Education Knowledge* 3, 11.
- Schoeneberger, P.J., Wysocki, D.A., Benham, E.C., Soil Survey Staff, 2012. *Field Book for Describing and Sampling Soils*. Version 3.0. Natural Resources Conservation Service, National Soil Survey Center, Lincoln, NE.
- Shen, Z., Törnqvist, T.E., Autin, W.J., Mateo, Z.R.P., Straub, K.M., Mauz, B., 2012. Rapid and widespread response of the Lower Mississippi River to eustatic forcing during the last glacial-interglacial cycle. *Geological Society of America Bulletin* 124, 690–704.
- Stahle, D.W., Fye, F.K., Cook, E.R., Griffin, R.D., 2007. Tree-ring reconstructed megadroughts over North America since AD 1300. *Climatic Change* 83, 133.

- Sweeney, M., Forman, S.L., McDonald, E.V., 2022. Contemporary and future dust emission processes and sources from gypsum- and quartz-dominated aeolian systems, New Mexico and Texas, USA. *Geology* **50**, 356–360.
- Taormina, R., Nordt, L., Bateman, M., 2022. Late quaternary alluvial history of the Brazos River in central Texas. *Quaternary International* **631**, 34–46.
- Tornqvist, T.E., Kidder, T.R., Autin, W.J., van der Borg, K., de Jong, A.F.M., Klerks, C.J.W., Snijders, E.M.A., Storms, J.E.A., van Dam, R.L., Wiemann, M.C., 1996. A revised chronology for Mississippi river subdeltas. *Science* **273**, 1693–1696.
- Waters, M.R., Keene, J.L., Prewitt, E.R., Everett, M.E., Laughlin, T., Stafford, T.W., 2021. Late Quaternary geology, archaeology, and geoarchaeology of Hall's Cave, Texas. *Quaternary Science Reviews* **274**, 107276.
- Waters, M.R., Nordt, L.C., 1995. Late Quaternary floodplain history of the Brazos River in east-central Texas. *Quaternary Research* **43**, 311–319.
- Werner, C.M., Mason, J.A., Hanson, P.R., 2011. Non-linear connections between dune activity and climate in the High Plains, Kansas and Oklahoma, USA. *Quaternary Research* **75**, 267–277.
- Wilkins, D.E., Currey, D.R., 1997. Timing and extent of Late Quaternary Paleolakes in the Trans-Pecos closed basin, west Texas and south-central New Mexico. *Quaternary Research* **47**, 306–315.
- Wintle, A.G., Murray, A.S., 2006. A review of quartz optically stimulated luminescence characteristics and their relevance in single-aliquot regeneration dating protocols. *Radiation Measurements* **41**, 369–391.
- Woodhouse, C.A., Lukas, J.J., Brown, P.M., 2002. Drought in the western Great Plains, 1845–56—impacts and implications. *Bulletin of the American Meteorological Society* **83**, 1485–1493.
- Wright, D.K., Forman, S.L., Waters, M.R., Ravesloot, J.C., 2011. Holocene eolian activation as a proxy for broad-scale landscape change on the Gila River Indian Community, Arizona. *Quaternary Research* **76**, 10–21.
- Yizhaq, H., Xu, Z., Ashkenazy, Y., 2020. The effect of wind speed averaging time on the calculation of sand drift potential: new scaling laws. *Earth and Planetary Science Letters* **544**, 116373.
- Zipper, S., Popescu, I., Compare, K., Zhang, C., Seybold, E.C., 2022. Alternative stable states and hydrological regime shifts in a large intermittent river. *Environmental Research Letters* **17**, 074005.